

## Joint Radial Velocity and Direct Imaging Planet Yield Calculations. II: Radial Velocity Scheduling and Cadence

2 PATRICK D. NEWMAN,<sup>1</sup> PETER PLAVCHAN,<sup>1</sup> JUSTIN CREPP,<sup>2</sup> SHANNON DULZ,<sup>2</sup> STEPHEN KANE,<sup>3</sup>  
3 RHONDA MORGAN,<sup>4</sup> CHRIS STARK,<sup>5</sup> GIJS MULDERS,<sup>6</sup> SARA SEAGER,<sup>7</sup> AND B. SCOTT GAUDI<sup>8</sup>

4 <sup>1</sup>*Department of Physics and Astronomy, George Mason University, 4400 University Drive, MSN 3F3, Fairfax, VA  
5 22030*

6 <sup>2</sup>*Department of Physics, University of Notre Dame, 225 Nieuwland Science Hall, Notre Dame, IN 46556, USA*

7 <sup>3</sup>*Department of Earth and Planetary Sciences, University of California, Riverside, CA 92521, USA*

8 <sup>4</sup>*Jet Propulsion Laboratory, California Institute of Technology, 4800 Oak Grove Dr., Pasadena, CA 91109, USA*

9 <sup>5</sup>*Space Telescope Science Institute*

10 <sup>6</sup>*Universidad Adolfo Ibez, Santiago de Chile*

11 <sup>7</sup>*MIT*

12 <sup>8</sup>*Department of Astronomy, The Ohio State University, 140 W. 18th Ave., Columbus, OH 43210*

13 (Dated: December 5, 2025)

## 14 Contents

15	1. Introduction	2
16	1.1. History	2
17	1.2. Motivation	3
18	2. Simulation Inputs	4
19	2.1. Target Catalogs	4
20	2.2. Telescope and Instrument Parameters	5
21	3. Radial Velocities	5
22	3.1. Stellar Properties	6
23	3.2. Exposure Time/Precision	13
24	3.3. Exposure Time Estimation	13
25	3.4. Atmospheric Effects	14
26	3.5. Stellar Activity	15
27	4. Dispatch Scheduler (Survey Simulations)	16
28	4.1. Target Weighting	17
29	5. Results (Overview)	19

30	5.1. Figure of merit: planet semi-amplitude sensitivity and detection SNR	19
31	5.2. Example Timeseries	19
32	6. Results (HWO target list)	20
33	6.1. Exposure Times and Observations	20
34	6.2. Exposure Times and Stellar Parameters	21
35	6.3. Right Ascension and Declination	22
36	6.4. Telluric Corrections	23
37	7. Results (HabEx target list)	24
38	8. Results (EPRV target list)	28
39	9. Discussion	33
40	9.1. Exposure Time Considerations	33
41	9.2. Comparisons to Other Exposure Time Calculators	33
42	9.2.1. ESPRESSO ETC	33
43	9.2.2. NEID ETC	34
44	9.3. Dispatch Scheduler considerations	36
45	9.4. Target Weighting	37
46	9.5. Do the different P-mode calculation methods affect yields?	39
47	9.6. Target List Comparison/Target Star Selection	45
48	9.7. Other/Uncompensated Noise	47
49	10. Conclusions	47

## 50           1. INTRODUCTION

### 51           1.1. *History*

52     While planet detection methods have greatly diversified since the first discoveries (Mayor & Queloz  
 53     1995), precision radial velocities remain a key component. The radial velocity method is still the  
 54     second most common detection method and a key technique to confirm and parameterize exoplanets.  
 55     It also probes a portion of the mass/radius - distance/period space that is inaccessible to other  
 56     methods, and has a clear path forwards to achieving the precision needed to detect and characterize  
 57     an earth-equivalent planet around a sun-equivalent star.

58     Simulating RV surveys to best determine direct imaging targets have a significant history, though  
 59     have generally stopped at around the then available precision. eg: Howard & Fulton (2016) performed  
 60     injection and recovery tests to determine yields and completeness, though were limited what sorts of  
 61     information could be supplied (since only ice giant and gas giant planets could be firmly detected).  
 62     Directly detecting terrestrial planets and providing mass estimates may soon be feasible, as opposed  
 63     to just limiting the parameter space. Bottom et al. (2013) looked across multiple spectral types and  
 64     wavelength ranges (including atmospheric windows), finding brighter, and therefore hotter, stars to  
 65     generally be more suitable. Less generally, the CARMENES radial velocity survey has developed a  
 66     highly detailed simulation system related to their spectrograph, telescope, and observation strategy.  
 67     (Garcia-Piquer et al. 2017) This simulation is used in part used for night to night planning.

Surveys are increasingly automated, though how to maximize planet yield is only beginning to be studied. [Handley et al. \(2024b\)](#)

The latest generation of Doppler RV facilities such as: NEID ([Halverson et al. 2016](#)), EXPRES ([Jurgenson et al. 2016](#)), ESPRESSO ([Pepe et al. 2021a](#)), and MAROON-X ([Seifahrt et al. 2018](#)) are reaching into 30 cm/s and lower single measurement precisions. It is currently expected that future ones will get down to around 10 cm/s, though significant obstacles remain.

## 1.2. Motivation

There remains considerable debate on the value of  $\eta_{\oplus}$  ([Bergsten et al. 2022](#); [Bryson et al. 2021](#); [Kunimoto & Matthews 2020](#); [Bryson et al. 2020](#); [Dulz et al. 2020](#); [Pascucci et al. 2019](#); [Hsu et al. 2019](#); [Zink & Hansen 2019](#); [Garrett et al. 2018](#); [Kopparapu et al. 2018](#); [Mulders et al. 2018](#); [Burke et al. 2015](#); [Foreman-Mackey et al. 2014](#); [Petigura et al. 2013](#); [Dong & Zhu 2013](#); [Youdin 2011](#); [Bonfils et al. 2013](#); [Kopparapu 2013](#); [Dressing & Charbonneau 2015](#); [Bergsten et al. 2023](#); [Kaminski et al. 2025](#); [Bryson et al. 2025](#); [Fernandes et al. 2025](#); [Silburt et al. 2015](#)), which will be difficult to resolve without characterization of the atmospheres of some tens of terrestrial planets.

Coronographic mission performance in particular is strongly affected by  $\eta_{\oplus}$ . Even for higher values, being able to skip the detection phase and proceed directly to characterization with an optimized observing schedule would improve performance.

Uninformed RV surveys generally choose bright and/or nearby stars due to having more photons to work with. Coronagraphic surveys also do so due to planet brightness, limited inner working angles, and greater angular scale. While early ground-based transit surveys focused on brighter stars, more recent and space-based ones have much reduced restrictions. They have found populations of exoplanets that are largely not amenable to detailed follow-up (especially atmospheric characterization).

Also, both (unlike transit) are looser in geometry requirements. The geometry means that there are nearby planets that are suitable for direct imaging that can be found with RVs, but not transits. The HabEx Interim Report ([Gaudi et al. 2018](#)) and related results point to a use for finding earth analogs that can be later characterized.

Even for a more general exoplanet demographics mission, masses from a precursor survey greatly assist in constraining atmospheric models. Both mass and radius are required to constrain exoplanet compositions. ([Rogers & Seager 2010](#)) In particular, more planet mass/radius measurements with smaller error bars and well quantified selection effects are needed to constrain the structure of the transition in between rocky and non-rocky planets. ([Rogers 2015](#))

Planet masses are also important for accurate atmospheric retrievals. Spectroscopy of planetary atmospheres can only find the mass to high precision in limited circumstances, ([de Wit & Seager 2013](#)) and characterizing secondary atmospheres has considerable uncertainty ([Changeat et al. \(2020\)](#)). Differing compositions (especially for super earths), can produce similar spectra for a wide array of masses. ([Batalha et al. 2017](#)) Clouds and high metallicity can make accurate atmospheric retrieval difficult without accurate mass estimates. For JWST, these are  $\pm 50\%$  for initial characterization, and  $\pm 20\%$  for spectroscopic errors to be more important than mass ones. ([Batalha et al. 2019](#)) Even in cases where atmospheric retrievals can be done with low quality mass priors, good orbit priors remain useful. ([Salvador et al. 2024](#))

In this paper, we present a multi-part pipeline for: generating a realistic radial velocity survey cadence for a given observing site telescope and properties, instrument and characteristics, desired radial velocity precision, and target list of nearby stars and associated known stellar parameters.

111 However, this paper is focused on the resulting cadence from this level of simulation fidelity compared  
 112 to more simplistic assumptions. We have developed this software to be re-usable and flexible for  
 113 considerations of other current and future radial velocity surveys, and the software is available online<sup>1</sup>.  
 114 For each target star/instrument/telescope/precision combination we estimate exposures times, and  
 115 resulting radial velocity precision from synthetic spectra after accounting for a typical airmass for  
 116 observations. We focus on: overall exposure times to get to desired EPRV precision targets, typical  
 117 numbers of observations per star as a result of the star’s position and exposure time, and figures  
 118 of merit for planet detection. In Section 2, we present the inputs to our simulation, and various  
 119 telescope and instruments considered, as well as the target lists considered. In Section 3, we present  
 120 how we calculate the estimated radial velocity precision and requisite exposure times. In Section 4,  
 121 we present how observations are scheduled in a simulated survey for a given a target prioritization  
 122 scheme. In Section 5, we present the results of the cadence of observations for the different scenarios  
 123 we consider. Additionally, we calculate a K/SNR figure of merit for these cadences. In Section 9,  
 124 we discuss the interesting highlights of our resulting cadences, and in Section 10 we present our  
 125 conclusions and plans for future work.

## 126 2. SIMULATION INPUTS

### 127 2.1. Target Catalogs

128 Testing our code has different requirements from pathfinder EPRV surveys, and the requirements  
 129 and target lists of the surveys are evolving over time. While most of our simulations are with a single  
 130 catalog, we construct multiple catalogs for some comparisons.

131 Our primary catalog uses Habitable Worlds Observatory’s ExEP list (as of 2023-07-26) was also  
 132 considered. This list (Mamajek & Stapelfeldt 2023, 2024) explicitly selects FGK stars and has cutoffs  
 133 for v·sini and  $R_{hk}$ . This catalog (hereafter called “HWO”) lacks explicit v·sini values, so we added  
 134 them from the literature. (Glebocki & Gnacinski 2005; Martínez-Arnáiz et al. 2010; Ammler-von Eiff  
 135 & Reiners 2012; Brewer et al. 2016; Luck 2017; Hojjatpanah et al. 2019)

136 Our initial star list comes from a modification of a version of the HabEx target list, which contains  
 137 72 Hipparcos stars. Given the source, this list has parameters somewhat different from a typical  
 138 uninformed RV survey. It does not select for low stellar activity, but for distance (consisting entirely  
 139 of stars within 5 parsecs). Constructing a catalog of the required stellar properties ( $T_{eff}$ , radius,  
 140 distance,  $v \cdot \sin(i)$ ,  $\log(g)$ ) was done via existing tables in VizieR (see table 2). This by necessity  
 141 makes it somewhat heterogeneous.

142 For the simulations, this target list was altered by: 1) Adding the companion star in a distant  
 143 binary (not in Hipparcos); 2) dropping an eclipsing binary; cutting all stars below -30 declination  
 144 (motivated by all sites currently being considered being in Arizona. Other target lists did not use this  
 145 cut, though the effect on the simulations was limited due to nature of the dispatch scheduler.). This  
 146 left 53 stars. Three sub-lists were also generated: the baseline “full” survey, a “deep” one containing  
 147 9 stars of particular interest to the HabEx team, and 47 stars that had no known planets at this time.  
 148 Many of the stars with known planets have hot jupiters, which are likely to preclude the existence  
 149 of habitable zone terrestrial planets.

<sup>1</sup> Available at [https://github.com/pdn4kd/dispatch\\_scheduler](https://github.com/pdn4kd/dispatch_scheduler)

This target list (“HabEx”) was run alongside synthetic catalogs for checking out code’s exposure times, coverage, and precision results to ensure that they were realistic.

A second run of this “HabEx” target list was also done without the declination cut for more directly getting exoplanet yields across our instrument types, sensitivities, and exposure timescales.

As a check, the catalog from Newman et al. (2023) (hereafter called the “EPRV target list”) is also used within our revised exposure considerations. This provides an “apples-to-apples” comparison with our previous work, by keeping the targets the same while varying the instruments and exposure parameters.

## 2.2. Telescope and Instrument Parameters

The simulations here all use telescopes in Arizona (see table 4). These all being northern hemisphere site would normally motivate a declination cut. We do not do so for this survey as a test of what the practical lower limit is. Our site locations are the standard ones listed for each telescope. Our weather is taken from Kitt Peak data (specifically WIYN, see figure 1), while MINERVA proper uses records from a survey of Mount Hopkins (Swift et al. 2015).

We assume constant throughput in our spectrographs, though with values that reflect their actual averages (table 1). These throughputs are at or below the low end of commonly reported values to compensate for those being peak values during nights with seeing. That is, they should reflect overall averages of the systems.

**Table 1.** Peak system throughputs for current EPRV spectrographs. These are higher than the averages used in the various architectures, as they largely do not account for performance variations from varying seeing and wavelength.

Spectrograph	Throughput	Source
ESPRESSO	10%	Pepe et al. (2021b)
EXPRES	9-15%	Blackman et al. (2020)
MAROON-X	7-8%, 11.5%	Seifahrt et al. (2020)
NEID	6%	Schwab et al. (2019)

## 3. RADIAL VELOCITIES

The radial velocity precision code<sup>2</sup> is an implementation and expansion of existing work (Beatty & Gaudi 2015). The major changes are: including macroturbulence when data is available, and aggregating radial velocity uncertainties across the visible/red/IR ranges if the spectrograph being simulated crosses them. This is expanded somewhat in that the telescope and instrument are simulated to the point of continuum atmospheric absorption/scattering, basic signal to noise considerations on each pixel, and exposure and readout times.

<sup>2</sup> Available at <https://github.com/pdn4kd/reimagined-palm-tree>

### 175 3.1. Stellar Properties

176 For the purpose of simulating RVs, stars are defined by:  $T_{eff}$ ,  $\log(g)$ ,  $v \cdot \sin(i)$ , metallicity, stellar  
177 radius, and distance. Effective temperature directly defines the atmosphere model used, while the  
178 rest scale RV content ( $\log(g)$ ,  $v \cdot \sin(i)$ , metallicity) or brightness (radius, distance).

179 While Beatty uses an estimate of macroturbulence based on effective temperature, some catalogs  
180 in the literature have measured this parameter (Brewer et al. 2016). Literature values are used where  
181 available.

**Table 2.** The HabEx stars and their properties used in these simulations.

RA (J2000)	Dec (J2000)	HIP	Vmag	Distance (pc)	Rstar	T <sub>eff</sub>	log(g)	Metallicity	V <sub>sini</sub>	Mstar	V <sub>mac</sub>
12.095738	5.280615	3765	5.74	7.4604597	0.74 <sup>1</sup>	4937 <sup>1</sup>	4.54 <sup>1</sup>	-0.22 <sup>1</sup>	0.7 <sup>1</sup>	0.69 <sup>1</sup>	1.7 <sup>1</sup>
12.276214	57.815186	3821	3.46	5.952735	1.05 <sup>1</sup>	5919 <sup>1</sup>	4.37 <sup>1</sup>	-0.21 <sup>1</sup>	0.5 <sup>1</sup>	0.94 <sup>1</sup>	4.2 <sup>1</sup>
25.624008	20.268505	7981	5.24	7.467702	0.81 <sup>1</sup>	5190 <sup>1</sup>	4.51 <sup>1</sup>	-0.03 <sup>1</sup>	0.1 <sup>1</sup>	0.78 <sup>1</sup>	2.0 <sup>1</sup>
26.017012	-15.93748	8102	3.49	3.647372	0.82 <sup>1</sup>	5333 <sup>1</sup>	4.6 <sup>1</sup>	-0.44 <sup>1</sup>	0.1 <sup>1</sup>	0.99 <sup>1</sup>	2.2 <sup>1</sup>
26.936811	63.8525	8362	5.63	9.976058	0.84 <sup>1</sup>	5344 <sup>1</sup>	4.54 <sup>1</sup>	0.01 <sup>1</sup>	0.8 <sup>1</sup>	0.89 <sup>1</sup>	2.3 <sup>1</sup>
41.049942	49.228447	12777	4.1	11.232169	1.31 <sup>1</sup>	6196 <sup>1</sup>	4.19 <sup>1</sup>	0.05 <sup>1</sup>	8.0 <sup>1</sup>	0.96 <sup>1</sup>	6.2 <sup>1</sup>
47.26675	49.613277	14632	4.05	10.534078	1.4 <sup>1</sup>	5938 <sup>1</sup>	4.18 <sup>1</sup>	0.13 <sup>1</sup>	3.4 <sup>1</sup>	1.07 <sup>1</sup>	4.3 <sup>1</sup>
55.81209	-9.763394	17378	3.52	9.043226	2.34 <sup>1</sup>	5037 <sup>1</sup>	3.75 <sup>1</sup>	0.15 <sup>1</sup>	0.1 <sup>1</sup>	1.11 <sup>1</sup>	3.4 <sup>1</sup>
63.818	-7.6528707	19849	4.43	5.0443907	0.83 <sup>1</sup>	5092 <sup>1</sup>	4.51 <sup>1</sup>	-0.2 <sup>1</sup>	0.5 <sup>1</sup>	0.8 <sup>1</sup>	1.9 <sup>1</sup>
72.460045	6.9612756	22449	3.19	8.025682	1.34 <sup>1</sup>	6398 <sup>1</sup>	4.27 <sup>1</sup>	0.05 <sup>1</sup>	16.4 <sup>1</sup>	1.21 <sup>1</sup>	8.5 <sup>1</sup>
79.78531	40.099052	24813	4.69	12.645422	1.28 <sup>1</sup>	5873 <sup>1</sup>	4.26 <sup>1</sup>	0.11 <sup>1</sup>	0.1 <sup>1</sup>	1.08 <sup>1</sup>	3.9 <sup>1</sup>
143.9146	35.810135	47080	5.4	11.17943	0.97 <sup>1</sup>	5499 <sup>1</sup>	4.44 <sup>1</sup>	0.27 <sup>1</sup>	2.8 <sup>1</sup>	0.95 <sup>1</sup>	2.6 <sup>1</sup>
175.26256	34.201637	56997	5.31	9.541075	0.86 <sup>1</sup>	5502 <sup>1</sup>	4.52 <sup>1</sup>	-0.07 <sup>1</sup>	2.2 <sup>1</sup>	0.9 <sup>1</sup>	2.6 <sup>1</sup>
176.62947	-40.500355	57443	4.89	9.239582	0.94 <sup>1</sup>	5672 <sup>1</sup>	4.51 <sup>1</sup>	-0.27 <sup>1</sup>	0.1 <sup>1</sup>	1.04 <sup>1</sup>	3.1 <sup>1</sup>
188.43561	41.35748	61317	4.24	8.371003	1.06 <sup>1</sup>	5884 <sup>1</sup>	4.42 <sup>1</sup>	-0.18 <sup>1</sup>	0.1 <sup>1</sup>	1.07 <sup>1</sup>	4.0 <sup>1</sup>
199.60132	-18.311195	64924	4.74	8.525149	0.97 <sup>1</sup>	5562 <sup>1</sup>	4.44 <sup>1</sup>	-0.03 <sup>1</sup>	0.8 <sup>1</sup>	0.93 <sup>1</sup>	2.8 <sup>1</sup>
223.34903	19.152798	72848	6.0	11.535356	0.84 <sup>1</sup>	5258 <sup>1</sup>	4.47 <sup>1</sup>	0.06 <sup>1</sup>	4.4 <sup>1</sup>	0.77 <sup>1</sup>	2.1 <sup>1</sup>
236.61089	7.353073	77257	4.42	11.753643	1.38 <sup>1</sup>	5901 <sup>1</sup>	4.22 <sup>1</sup>	0.04 <sup>1</sup>	2.0 <sup>1</sup>	1.15 <sup>1</sup>	4.1 <sup>1</sup>
272.4059	38.457775	88972	6.38	11.097548	0.8 <sup>1</sup>	4970 <sup>1</sup>	4.51 <sup>1</sup>	-0.1 <sup>1</sup>	0.1 <sup>1</sup>	0.76 <sup>1</sup>	1.8 <sup>1</sup>
293.08997	69.66118	96100	4.67	5.76668	0.79 <sup>1</sup>	5242 <sup>1</sup>	4.56 <sup>1</sup>	-0.21 <sup>1</sup>	0.5 <sup>1</sup>	0.81 <sup>1</sup>	2.1 <sup>1</sup>
298.8283	6.4067636	98036	3.71	13.70802	3.17 <sup>1</sup>	5081 <sup>1</sup>	3.55 <sup>1</sup>	-0.11 <sup>1</sup>	0.1 <sup>1</sup>	1.3 <sup>1</sup>	3.5 <sup>1</sup>
303.82245	-27.032976	99825	5.73	8.823789	0.82 <sup>1</sup>	5071 <sup>1</sup>	4.5 <sup>1</sup>	0.05 <sup>1</sup>	1.2 <sup>1</sup>	0.78 <sup>1</sup>	1.9 <sup>1</sup>
331.75278	25.345112	109176	3.77	11.756408	1.42 <sup>1</sup>	6565 <sup>1</sup>	4.25 <sup>1</sup>	-0.05 <sup>1</sup>	0.1 <sup>1</sup>	1.31 <sup>1</sup>	11.2 <sup>1</sup>
5.0177503	-64.874794	1599	4.23	8.592542	1.055 <sup>2</sup>	5948 <sup>2</sup>	4.46 <sup>2</sup>	-0.18 <sup>2</sup>	3.0 <sup>2</sup>	1.176 <sup>2</sup>	...
6.4378004	-77.25424	2021	2.82	7.474959	1.802 <sup>2</sup>	5873 <sup>2</sup>	4.08 <sup>2</sup>	-0.09 <sup>2</sup>	4.0 <sup>2</sup>	1.433 <sup>2</sup>	...
9.840858	21.250473	3093	5.88	11.107409	0.879 <sup>2</sup>	5221 <sup>2</sup>	4.45 <sup>2</sup>	0.16 <sup>2</sup>	1.1 <sup>2</sup>	0.799 <sup>2</sup>	...
24.199345	41.40546	7513	4.1	13.468014	1.573 <sup>2</sup>	6213 <sup>2</sup>	4.25 <sup>2</sup>	0.12 <sup>2</sup>	9.6 <sup>2</sup>	1.62 <sup>2</sup>	...
39.02039	6.8868704	12114	5.79	7.208766	0.7348 <sup>2</sup>	4866 <sup>2</sup>	4.66 <sup>2</sup>	0.0 <sup>2</sup>	2.9 <sup>2</sup>	0.909 <sup>2</sup>	...
43.13387	-12.769714	13402	6.05	10.380981	0.7532 <sup>2</sup>	5236 <sup>2</sup>	4.59 <sup>2</sup>	0.11 <sup>2</sup>	4.9 <sup>2</sup>	0.811 <sup>2</sup>	...
49.44235	-62.57532	15330	5.53	12.119742	0.9062 <sup>2</sup>	5699 <sup>2</sup>	4.58 <sup>2</sup>	-0.22 <sup>2</sup>	2.9 <sup>2</sup>	1.128 <sup>2</sup>	...
49.553413	-62.506363	15371	5.24	12.078753	0.9721 <sup>2</sup>	5845 <sup>2</sup>	4.54 <sup>2</sup>	-0.23 <sup>2</sup>	2.6 <sup>2</sup>	1.192 <sup>2</sup>	...
49.8404	3.370198	15457	4.84	9.159186	0.917 <sup>2</sup>	5742 <sup>2</sup>	4.49 <sup>2</sup>	0.1 <sup>2</sup>	5.2 <sup>2</sup>	0.948 <sup>2</sup>	...
49.98188	-43.069782	15510	4.26	6.059871	0.928 <sup>2</sup>	5401 <sup>2</sup>	4.62 <sup>2</sup>	-0.23 <sup>2</sup>	1.5 <sup>2</sup>	1.3 <sup>2</sup>	...
75.20417	-5.7536755	23311	6.22	8.813679	0.7579 <sup>2</sup>	4827 <sup>2</sup>	4.69 <sup>2</sup>	0.3 <sup>2</sup>	1.7 <sup>2</sup>	1.031 <sup>2</sup>	...
92.56031	-74.753044	29271	5.08	10.148163	0.9729 <sup>2</sup>	5587 <sup>2</sup>	4.5 <sup>2</sup>	0.05 <sup>2</sup>	1.7 <sup>2</sup>	1.103 <sup>2</sup>	...
103.07521	-5.173713	32984	6.58	8.7001915	0.665 <sup>2</sup>	4758 <sup>2</sup>	4.92 <sup>2</sup>	-0.01 <sup>2</sup>	1.8 <sup>2</sup>	1.34 <sup>2</sup>	...
114.82549	5.224993	37279	0.4	3.4973595	1.919 <sup>2</sup>	6543 <sup>2</sup>	3.99 <sup>2</sup>	0.03 <sup>2</sup>	5.7 <sup>2</sup>	1.32 <sup>2</sup>	...
157.65659	55.980537	51459	4.82	12.850167	1.12 <sup>2</sup>	6126 <sup>2</sup>	4.34 <sup>2</sup>	-0.05 <sup>2</sup>	2.1 <sup>2</sup>	0.994 <sup>2</sup>	...
177.67383	1.7647179	57757	3.59	10.900371	1.639 <sup>2</sup>	6161 <sup>2</sup>	4.22 <sup>2</sup>	0.16 <sup>2</sup>	4.0 <sup>2</sup>	1.61 <sup>2</sup>	...
178.24487	37.718678	57939	6.42	9.156671	0.659 <sup>2</sup>	4950 <sup>2</sup>	4.65 <sup>2</sup>	-1.16 <sup>2</sup>	0.5 <sup>2</sup>	0.716 <sup>2</sup>	...
197.9683	27.878183	64394	4.23	9.154994	1.063 <sup>2</sup>	6075 <sup>2</sup>	4.57 <sup>2</sup>	0.04 <sup>2</sup>	4.4 <sup>2</sup>	1.54 <sup>2</sup>	...
209.38358	61.492863	68184	6.49	10.104072	0.802 <sup>2</sup>	4757 <sup>2</sup>	4.58 <sup>2</sup>	0.1 <sup>2</sup>	1.3 <sup>2</sup>	0.89 <sup>2</sup>	...
224.36667	-21.415476	73184	5.72	5.905977	0.6754 <sup>2</sup>	4744 <sup>2</sup>	4.76 <sup>2</sup>	0.1 <sup>2</sup>	2.6 <sup>2</sup>	0.951 <sup>2</sup>	...
239.11327	15.661617	78072	3.85	11.120996	1.447 <sup>2</sup>	6262 <sup>2</sup>	4.18 <sup>2</sup>	-0.14 <sup>2</sup>	10.9 <sup>2</sup>	1.16 <sup>2</sup>	...
249.08937	-2.3245835	81300	5.77	9.778039	0.791 <sup>2</sup>	5277 <sup>2</sup>	4.57 <sup>2</sup>	0.05 <sup>2</sup>	2.2 <sup>2</sup>	0.853 <sup>2</sup>	...

**Table 2** continued on next page

**Table 2** (*continued*)

RA (J2000)	Dec (J2000)	HIP	Vmag	Distance (pc)	Rstar	T <sub>eff</sub>	log(g)	Metallicity	V <sub>sini</sub>	Mstar	V <sub>mac</sub>
259.76596	-46.636234	84720	5.47	8.786574	0.777 <sup>2</sup>	5256 <sup>2</sup>	4.61 <sup>2</sup>	-0.27 <sup>2</sup>	0.3 <sup>2</sup>	0.901 <sup>2</sup>	...
302.1817	-66.18207	99240	3.55	6.1076164	1.178 <sup>2</sup>	5590 <sup>2</sup>	4.31 <sup>2</sup>	0.26 <sup>2</sup>	2.3 <sup>2</sup>	1.045 <sup>2</sup>	...
302.79974	-36.10121	99461	5.32	6.051803	0.7422 <sup>2</sup>	4922 <sup>2</sup>	4.58 <sup>2</sup>	-0.33 <sup>2</sup>	2.7 <sup>2</sup>	0.766 <sup>2</sup>	...
348.32074	57.168354	114622	5.57	6.525711	0.751 <sup>2</sup>	4835 <sup>2</sup>	4.56 <sup>2</sup>	0.09 <sup>2</sup>	1.8 <sup>2</sup>	0.749 <sup>2</sup>	...
53.232685	-9.458262	16537	3.72	3.218021	0.7188 <sup>2</sup>	5146 <sup>2</sup>	4.57 <sup>2</sup>	0.0 <sup>2</sup>	2.4 <sup>2</sup>	0.708 <sup>2</sup>	...
86.11579	-22.448381	27072	3.59	8.969415	1.2 <sup>3</sup>	6241 <sup>4</sup>	4.19 <sup>4</sup>	-0.16 <sup>4</sup>	8.9 <sup>5</sup>	1.4 <sup>6</sup>	...
208.67116	18.397717	67927	2.68	11.341726	2.19 <sup>3</sup>	6201.8 <sup>7</sup>	3.96 <sup>7</sup>	0.13 <sup>7</sup>	11.3 <sup>5</sup>	1.15 <sup>8</sup>	...
247.11726	-70.084404	80686	4.9	12.105072	0.99 <sup>3</sup>	5963 <sup>9</sup>	4.45 <sup>9</sup>	-0.16 <sup>9</sup>	2.4 <sup>5</sup>	1.2 <sup>6</sup> <sup>8</sup>	...
4.59542	44.02278	1475	8.13	3.5679882	0.388 <sup>10</sup>	3603 <sup>10</sup>	4.83 <sup>10</sup> <sup>99</sup>	-0.3 <sup>10</sup>	0.6 <sup>11</sup>	0.398 <sup>10</sup>	...
4.60779	44.02734	1475B	11.04	3.5679882	0.1923 <sup>10</sup>	3218 <sup>10</sup>	4.92 <sup>12</sup>	-0.3 <sup>10</sup>	0.1 <sup>11</sup>	0.159 <sup>10</sup>	...
34.26346	34.22423	10644	4.84	10.845987	0.98 <sup>3</sup>	5597 <sup>13</sup>	3.92 <sup>13</sup>	-0.41 <sup>13</sup>	8.6 <sup>5</sup>	1.125 <sup>8</sup> <sup>99</sup>	...
76.37773	-57.472702	23693	4.71	11.650938	1.3 <sup>3</sup>	6069 <sup>9</sup>	4.45 <sup>9</sup>	-0.25 <sup>9</sup>	17.3 <sup>5</sup>	1.2 <sup>6</sup> <sup>8</sup>	...
77.91909	-45.018414	24186	8.86	3.9175744	0.43 <sup>3</sup>	3524 <sup>9</sup>	4.87 <sup>9</sup>	-0.5 <sup>9</sup>	5.4 <sup>5</sup>	0.49 <sup>14</sup>	...
82.86415	-3.677229	25878	7.97	5.6908717	0.5735 <sup>15</sup>	3850 <sup>15</sup>	4.7 <sup>12</sup>	0.0 <sup>12</sup>	2.73 <sup>16</sup>	0.633 <sup>10</sup>	...
92.64423	-21.864643	29295	8.15	5.7740054	0.695 <sup>16</sup>	3522 <sup>16</sup>	5.0 <sup>17</sup>	0.06 <sup>16</sup>	1.6 <sup>5</sup>	0.49 <sup>14</sup>	...
152.84225	49.454235	49908	6.6	4.8728194	0.6398 <sup>15</sup>	4176 <sup>15</sup>	4.55 <sup>12</sup>	-0.05 <sup>12</sup>	2.5 <sup>5</sup>	0.707 <sup>10</sup>	...
165.83414	35.96988	54035	7.49	2.54842	0.3924 <sup>15</sup>	3532 <sup>15</sup>	4.82 <sup>12</sup>	-0.4 <sup>12</sup>	1.6 <sup>5</sup>	0.386 <sup>10</sup>	...
217.42896	-62.679485	70890	11.01	1.2947832	0.141 <sup>18</sup>	3054 <sup>19</sup>	5.21 <sup>99</sup>	0.19 <sup>20</sup>	0.0864 <sup>21</sup>	0.118	...
259.05566	-26.546146	84478	6.33	5.9680114	0.72 <sup>3</sup>	4380 <sup>12</sup>	4.71 <sup>12</sup>	-0.27 <sup>12</sup>	3.3 <sup>5</sup>	0.67 <sup>8</sup>	...
297.69583	8.868322	97649	0.76	5.142975	1.5 <sup>3</sup>	7550 <sup>9</sup>	4.13 <sup>9</sup>	-0.24 <sup>9</sup>	211.0 <sup>5</sup>	1.74 <sup>22</sup>	...
316.72476	38.749416	104214	5.2	3.482743	0.728 <sup>3</sup>	4242 <sup>12</sup>	4.7 <sup>12</sup>	-0.38 <sup>12</sup>	2.0 <sup>5</sup>	0.67 <sup>8</sup>	...
316.73026	38.742054	104217	6.05	3.5036085	0.601 <sup>15</sup>	4025 <sup>15</sup>	4.49 <sup>13</sup>	-0.41 <sup>13</sup>	1.6 <sup>5</sup>	0.641 <sup>10</sup>	...
319.31363	-38.867363	105090	6.69	3.9467971	0.72 <sup>3</sup>	3796 <sup>23</sup>	4.55 <sup>23</sup>	-0.62 <sup>23</sup>	0.9 <sup>5</sup>	0.58	...
321.61087	-65.366196	105858	4.21	9.21659	1.0 <sup>3</sup>	6150 <sup>24</sup>	4.35 <sup>24</sup>	-0.66 <sup>24</sup>	3.4 <sup>5</sup>	0.932	...
330.84024	-56.785976	108870	4.69	3.6263416	0.84 <sup>3</sup>	4500 <sup>9</sup>	4.7 <sup>9</sup>	0.04 <sup>9</sup>	1.4 <sup>5</sup>	0.67 <sup>8</sup>	...
344.10022	-31.565567	113283	6.48	7.6370854	0.65 <sup>25</sup>	4555 <sup>9</sup>	4.53 <sup>9</sup>	-0.01 <sup>9</sup>	2.6 <sup>5</sup>	0.77	...
346.46683	-35.85307	114046	7.35	3.2905562	0.468 <sup>10</sup>	3688 <sup>10</sup>	4.79 <sup>10</sup> <sup>99</sup>	-0.06 <sup>10</sup>	0.9 <sup>5</sup>	0.495 <sup>10</sup>	...

**Table 3.** The HWO stars and their properties used in these simulations.

RA (J2000)	Dec (J2000)	HIP	Vmag	Distance (pc)	Rstar	T <sub>eff</sub>	log(g)	Metallicity	V <sub>sini</sub>	Mstar
129.7987692	65.0209064	42438	5.63	14.4388	0.946	5893	4.53	-0.07	9.3	1.08
137.2127933	33.8822184	44897	5.962	18.9498	1.045	5992	4.5	0.04	4.4	1.08
147.1473806	46.0210074	48113	5.086	18.8226	1.604	5893	4.12	0.1	2.9	1.08
157.6565803	55.9805388	51459 A	4.82	12.9452	1.111	6164	4.43	-0.12	8.6	1.18
178.2448639	37.7186817	57939	6.427	9.1718	0.6	5057	4.64	-1.33	2.9	0.85
188.01761	-16.1960052	61174	4.297	18.2437	1.517	6871	4.242	-0.06	66.8	1.44
188.4356011	41.3574781	61317	4.26	8.4727	1.034	5878	4.42	-0.2	2.8	1.08
198.0132679	-37.8030222	64408	4.847	20.4628	2.116	5688	3.92	0.16	2.7	0.99

**Table 3** continued on next page

<sup>1</sup> Brewer et al. (2016), <sup>2</sup> Valenti & Fischer (2005), <sup>3</sup> Pasinetti Fracassini et al. (2001), <sup>4</sup> Rich et al. (2017), <sup>5</sup> Glebocki & Gnacinski (2005), <sup>6</sup> Assumed, <sup>7</sup> Kunder et al. (2017), <sup>8</sup> ISBN 0199697140, <sup>9</sup> (Soubiran et al. 2016), <sup>10</sup> Mann et al. (2015), <sup>11</sup> Newton et al. (2016), <sup>12</sup> (Prugniel et al. 2011) , <sup>13</sup> (Prugniel et al. 2007), <sup>14</sup> Kaltenegger & Traub (2009), <sup>15</sup> Newton et al. (2015), <sup>16</sup> Houdebine (2010), <sup>17</sup> Rajpurohit et al. (2013), <sup>18</sup> Demory et al. (2009), <sup>19</sup> Boyajian et al. (2012), <sup>20</sup> Edvardsson et al. (1993), <sup>21</sup> Kiraga & Stepień (2007), <sup>22</sup> Adelman (2004), <sup>23</sup> Koleva & Vazdekis (2012), <sup>24</sup> Ramírez et al. (2013), <sup>25</sup> Gáspár et al. (2016), <sup>99</sup> Calculated

**Table 3** (*continued*)

RA (J2000)	Dec (J2000)	HIP	Vmag	Distance (pc)	Rstar	T <sub>eff</sub>	log(g)	Metallicity	V <sub>sini</sub>	Mstar
218.6700724	29.7451271	71284	4.465	15.756	1.306	6745	4.26	-0.41	8.1	1.39
230.4506246	-48.3176305	75181	5.655	14.7391	1.046	5685	4.37	-0.34	2.4	1.02
238.168921	42.4515175	77760	4.608	15.8975	1.742	5820	4.06	-0.47	3.4	1.08
239.1132612	15.6616168	78072	3.843	11.2537	1.47	6285	4.14	-0.18	9.9	1.25
246.0053797	-39.1929805	80337	5.37	12.8923	0.968	5868	4.53	0.05	2.2	1.07
266.0362631	-51.8340532	86796	5.124	15.6042	1.383	5761	4.25	0.29	3.8	1
271.5988313	-36.0197863	88694 A	5.949	17.1146	0.98	5892	4.38	-0.05	7.3	1.08
272.4059009	38.4577772	88972	6.377	11.0959	0.794	5028	4.5	-0.18	0.6	0.78
291.2424999	11.9444135	95447	5.169	14.922	1.393	5593	4.19	0.38	1.9	0.95
296.6066669	33.7275982	97295 A	5.005	20.9857	1.503	6455	4.26	0.03	8.2	1.29
304.3805338	66.853689	100017	5.922	17.4813	0.999	5930	4.48	-0.1	2.7	1.08
316.730266	38.742044	104217	6.043	3.4964	0.551	4107	4.47	-0.21	1.8	0.63
330.8402234	-56.7859786	108870	4.674	3.6384	0.728	4641	4.29	-0.13	1.4	0.72
2.9334212	-35.1331147	950	5.241	21.7191	1.375	6495	4.3	-0.11	10	1.33
12.5316207	-10.6443289	3909	5.176	15.923	1.153	6208	4.39	-0.12	3.9	1.21
24.9492196	-56.1933179	7751 A	5.764	8.1894	0.775	5025	4.6	-0.24	1.8	0.78
25.6240105	20.2685127	7981	5.241	7.6439	0.828	5204	4.49	-0.04	0.1	0.85
34.7437699	-25.9456872	10798	6.336	12.8347	0.762	5401	4.59	-0.49	2.7	0.94
49.4423477	-62.5753201	15330	5.513	12.0447	0.911	5710	4.5	-0.23	2.7	1.01
49.9818788	-43.069782	15510	4.258	6.0414	0.913	5432	4.46	-0.39	0.9	0.97
56.7120305	-23.2497228	17651	4.21	17.7847	1.678	6685	4.141	0.08	13.2	1.33
71.9012154	-16.9344557	22263	5.489	13.24	0.962	5833	4.49	0	2.9	1.04
84.2911952	-80.4691207	26394	5.666	18.2874	1.153	5982	4.39	0.09	2.7	1.08
86.1157942	-22.4483855	27072 A	3.596	8.905	1.28	6313	4.35	-0.08	7.2	1.23
101.6847372	43.5774246	32480	5.252	16.6106	1.224	6066	4.38	0.11	3.6	1.14
103.0752106	-5.1737127	32984 A	6.562	8.7447	0.687	4767	4.54	0.02	2.7	0.79
105.9888134	-43.608035	34065	5.56	17.0593	1.213	5790	4.33	-0.22	3.6	1.04
108.9589132	47.2399634	35136	5.559	16.8518	1.157	5902	4.32	-0.32	2.9	1.14
103.8277765	25.3756954	33277	5.763	17.4047	1.08	5924	4.44	-0.12	2.9	1.08
219.9020583	-60.8339927	71683	0.002	1.3319	1.231	5776	4.3	0.2	3.2	1.11
240.2610854	33.303511	78459	5.41	17.5108	1.328	5812	4.25	-0.22	1.5	0.97
319.3136211	-38.8673622	105090	6.69	3.9696	0.64	3874	4.78	-0.01	0.9	0.59
12.0957332	5.2806137	3765	5.729	7.4352	0.728	5007	4.62	-0.26	1.8	0.78
72.4600454	6.9612745	22449	3.184	8.0684	1.321	6443	4.3	0.03	15.3	1.25
327.0656298	-47.3036161	107649	5.575	15.5589	1.039	5935	4.41	-0.03	1.8	1.08
156.0987749	-74.0316121	50954	3.99	16.2232	1.587	6905	4.228	0.05	40.7	1.43
199.6013083	-18.3111938	64924	4.735	8.5344	0.982	5552	4.41	-0.01	1.8	0.97
236.6108925	7.3530687	77257	4.422	11.9159	1.356	5898	4.18	-0.01	3.3	1.09
303.8224641	-27.0329754	99825	5.73	8.8116	0.818	5087	4.48	0.03	0.6	0.77
1.6532667	29.0215035	544	6.093	13.7662	0.889	5491	4.55	0.11	3.6	0.94
49.553412	-62.5063624	15371	5.232	12.0394	0.983	5847	4.46	-0.23	2.7	1.07
175.2625678	34.2016338	56997	5.308	9.5762	0.862	5491	4.54	-0.05	2.3	0.94
259.0556767	-26.5461491	84478	6.295	5.9537	0.66	4476	4.57	-0.21	3.3	0.68
261.2504073	67.306708	85235	6.443	12.7919	0.761	5302	4.58	-0.46	1.3	0.87
311.5238859	-25.2708975	102485	4.137	14.6334	1.42	6638	4.238	0.04	42.2	1.33
332.5365841	-32.5484084	109422	4.94	18.4579	1.405	6364	4.2	0.1	12.6	1.25
80.6397108	79.2311507	25110	5.08	20.7858	1.496	6354	4.2	0.12	11.7	1.21

**Table 3** continued on next page

**Table 3** (*continued*)

RA (J2000)	Dec (J2000)	HIP	Vmag	Distance (pc)	Rstar	T <sub>eff</sub>	log(g)	Metallicity	V <sub>sini</sub>	Mstar
85.334732	53.481058	26779	6.2	12.2701	0.843	5226	4.52	0.1	3	0.88
133.5747796	-5.4344595	43726	6.008	16.8465	0.983	5780	4.49	0.1	2.4	1.02
226.8252747	24.8691943	73996	4.94	19.536	1.451	6435	4.19	-0.02	43	1.33
273.4743034	64.3972849	89348	4.99	23.1569	1.624	6473	4.09	-0.29	9.7	1.33
349.1762648	53.2134748	114924	5.58	20.6102	1.286	6084	4.19	0.03	5.4	1.18
94.1109129	12.2721632	29800	5.04	19.5879	1.364	6480	4.307	-0.03	17.1	1.33
145.5600675	-23.9155672	47592	4.914	14.9515	1.233	6163	4.34	-0.06	5.3	1.14
224.36667	-21.4154798	73184	5.724	5.8864	0.732	4632	4.49	0.02	3.5	0.72
293.0899592	69.6611766	96100	4.672	5.7639	0.782	5298	4.52	-0.21	1.8	0.87
75.2041639	-5.7536734	23311	6.202	8.844	0.776	4810	4.46	0.31	1.4	0.75
81.106097	17.3835351	25278	5.009	14.5792	1.182	6131	4.29	0.01	14.4	1.18
49.8404013	3.3701986	15457	4.85	9.2762	0.946	5709	4.51	0.04	4.5	0.98
118.0652624	-34.7054399	38423 A	5.085	18.3274	1.246	6525	4.276	-0.08	48.4	1.33
41.2758283	-18.5726228	12843	4.465	14.2764	1.345	6330	4.36	0.07	27.3	1.21
321.6108541	-65.3661981	105858	4.229	9.2584	1.086	6095	4.3	-0.7	3.4	1.14
26.9368101	63.8525031	8362	5.626	10.0411	0.834	5358	4.48	0.03	0.9	0.9
272.6089738	-62.00222	89042	5.469	17.7532	1.238	5951	4.29	-0.07	4.2	1.08
5.0177443	-64.8747937	1599	4.223	8.6071	1.063	5932	4.43	-0.21	4.9	1.11
60.6531011	-0.2689222	18859	5.361	18.707	1.206	6268	4.34	0.1	17.7	1.21
62.1525715	38.0397386	19335	5.522	21.1919	1.242	6381	4.61	0.19	16.2	1.18
25.6221438	-53.740831	7978	5.52	17.3488	1.095	6155	4.44	-0.04	5.4	1.14
354.9876724	5.626291	116771	4.132	13.7137	1.591	6200	4.15	-0.14	6.3	1.21
265.8574731	-21.6831941	86736	4.86	17.6523	1.335	6404	4.26	-0.11	11.7	1.33
300.9058545	29.8968035	98767	5.745	16.0035	1.162	5563	4.32	0.22	0.8	0.96
348.320729	57.1683566	114622	5.54	6.5418	0.723	4874	4.56	0.06	1.8	0.75
13.2674852	61.123972	4151	4.8	18.8007	1.656	6105	4.11	0.05	8.6	1.18
349.2403645	-62.0011978	114948	5.655	20.4426	1.16	6280	4.37	-0.03	7.6	1.25
18.7963393	-45.5316646	5862	4.966	15.2609	1.263	6110	4.34	0.16	4.7	1.14
302.1817036	-66.1820674	99240	3.556	6.0993	1.198	5576	4.29	0.35	2	0.94
165.8341451	35.9698823	54035	7.421	2.5461	0.363	3601	4.87	-0.42	1.6	0.44
209.3835765	61.4928612	68184	6.488	10.0672	0.759	4867	4.56	0.2		0.75
26.0170131	-15.9374799	8102	3.496	3.6522	0.826	5356	4.53	-0.51	0.9	0.94
87.1455844	-4.0946449	27435	5.973	15.2104	0.922	5731	4.47	-0.22	2.7	1.02
249.0893737	-2.324587	81300	5.764	9.8939	0.818	5262	4.52	0.03	1.6	0.87
125.0160865	27.217705	40843	5.13	18.2233	1.32	6269	4.3	-0.28	4.3	1.25
316.7247483	38.7494173	104214	5.211	3.4966	0.637	4441	4.51	-0.13	1.8	0.68
130.8251265	-38.8823808	42808	6.556	11.1917	0.753	4992	4.6	0.01	2.7	0.76
301.3865229	-67.3208961	98959	6.07	17.9323	1.033	5730	4.42	-0.19	1.8	1.02
11.4399705	-47.5519841	3583 A	5.795	15.0487	0.924	5887	4.65	-0.04	3.6	0.98
55.8120856	-9.7633919	17378	3.537	9.0888	2.245	5045	3.78	0.09	1	0.87
176.6294689	-40.5003572	57443 A	4.893	9.3195	0.97	5618	4.44	-0.31	2.7	1.02
164.8665531	40.4302557	53721	5.037	13.8875	1.21	5880	4.3	0.02	3.1	1.07
260.1648644	32.4677439	84862	5.385	14.5863	1.163	5704	4.33	-0.39	1.6	0.94
346.4668158	-35.8530709	114046	7.33	3.2871	0.47	3680	4.88	-0.22	0.9	0.49
43.1338674	-12.7697133	13402	6.038	10.3605	0.78	5199	4.55	0.07	6.2	0.82
93.7119848	19.1564479	29650	5.2	21.7763	1.335	6539	4.29	0.03	8.6	1.29
79.7853144	40.0990514	24813	4.705	12.5625	1.279	5854	4.24	0.06	1.3	1.08

**Table 3** continued on next page

**Table 3** (*continued*)

RA (J2000)	Dec (J2000)	HIP	Vmag	Distance (pc)	Rstar	T <sub>eff</sub>	log(g)	Metallicity	V <sub>sini</sub>	Mstar
191.2475207	39.2789162	62207	5.958	17.5565	1.004	5889	4.38	-0.53	1.8	1.14
197.9683076	27.878184	64394	4.23	9.1975	1.079	5996	4.42	0.06	4.5	1.11
152.8422498	49.4542364	49908	6.55	4.8706	0.636	4097	4.64	0.21	2.7	0.63
6.4377932	-77.2542461	2021	2.82	7.4588	1.844	5806	4	-0.12	3.4	1.08
124.599779	-12.6321714	40693	5.951	12.5794	0.883	5423	4.53	-0.03	2.2	0.93
243.9052928	-8.3694395	79672	5.496	14.1369	1.041	5785	4.43	0.03	2.7	1.02
177.6738271	1.7647226	57757	3.602	10.929	1.679	6123	4.13	0.13	3.6	1.14
326.1305414	14.7719398	107350	5.942	18.133	1.006	5939	4.45	-0.06	9.9	1.08
128.2145653	-31.5008514	41926	6.378	12.1643	0.765	5261	4.56	-0.39	1.8	0.85
344.100219	-31.565564	113283	6.446	7.6015	0.697	4601	4.68	0.04	2.6	0.72
40.6394444	-50.8002931	12653	5.395	17.3572	1.158	6157	4.43	0.15	5.4	1.14
53.2326854	-9.458261	16537	3.718	3.2198	0.746	5098	4.55	-0.08	1.9	0.78
54.2182654	0.4016645	16852	4.291	13.9204	1.623	5996	4.1	-0.08	3.7	1.14
265.0992732	-49.4155831	86486	4.762	20.9624	1.621	6620	4.161	-0.22	14	1.39
2.8160752	-15.4679779	910	4.895	18.8861	1.505	6190	4.09	-0.36	4.8	1.18
47.2667471	49.6132784	14632	4.05	10.5774	1.404	5952	4.22	0.09	3.6	1.08
137.5981111	67.1340172	45038 A	4.809	20.5169	1.68	6325	4.07	-0.02	5.8	1.21
157.8409203	-53.7154836	51523	4.897	22.0616	1.845	6155	3.83	-0.4	8.3	1.16
222.8474519	19.1004499	72659 A	4.54	6.7536	0.823	5487	4.54	-0.14	3.5	0.96
258.8374326	-26.602826	84405 B	5.11	5.9478	0.725	5144	4.59	-0.22	4.4	0.85
259.7659898	-46.6362334	84720 A	5.472	8.7911	0.817	5235	4.56	-0.35	1.8	0.9
260.2515605	-21.1129364	84893 A	4.389	17.5187	1.484	6756	4.254	-0.25	18.9	1.44
314.1972153	-26.2963779	103389	5.709	21.1021	1.182	6270	4.35	-0.01	13.7	1.2
336.2348695	-57.7974559	110649 A	5.318	20.3398	1.717	5660	4.13	-0.03	1.8	1.02
338.6734824	-20.7082158	111449 A	5.21	23.0205	1.419	6605	4.274	0.03	34.7	1.35
9.8408558	21.2504758	3093 A	5.863	11.1081	0.898	5203	4.47	0.14	1.8	0.86
41.0499442	49.2284485	12777 A	4.1	11.1501	1.273	6263	4.39	0.01	8.6	1.21
48.0188742	-28.987622	14879 A	3.8	13.999	1.79	6195	3.95	-0.22	5.7	1.25
63.8179984	-7.6528697	19849 A	4.415	5.0098	0.809	5133	4.52	-0.29	0.9	0.86
119.4454762	-60.3030719	38908 A	5.592	16.1718	1.052	5997	4.52	-0.31	2.7	1.11
18.9420379	-68.8759448	5896 A	4.912	23.2606	1.588	6436	4.021	0.03	61.1	1.35
297.7568487	10.4157201	97675 A	5.122	19.4881	1.491	6134	4.22	0.12	2.8	1.25
92.5603024	-74.753044	29271 A	5.076	10.2129	0.99	5594	4.46	0.1	2.3	0.96
236.8712542	-37.9163119	77358 A	6.012	15.2465	0.959	5602	4.47	0.1	1.8	0.96
271.3644289	2.498947	88601 B	6.061	5.1225	0.674	4475	4.64	0.03	3.7	0.78
24.9481863	-56.1964481	7751 B	5.876	8.1965	0.703	5111	4.63	-0.19	2.5	0.77
112.4831549	49.6724594	36439	5.35	20.4021	1.292	6349	4.29	-0.28	9.7	1.16
157.7696164	82.5586517	51502 A	5.25	22.7302	1.316	6758	4.389	-0.16	94.2	1.39
182.1034022	-24.7288751	59199 A	4.025	14.9365	1.439	6990	4.192	-0.13	23.8	1.5
271.363535	2.5001463	88601 A	4.22	5.1133	0.865	5298	4.52	0.06	4.3	0.88
86.1105697	-22.4218374	27072 B	6.142	8.8916	0.719	4950	4.33	-0.14	4.3	0.81
154.93403	19.4709128	50564	4.792	21.2199	1.669	6410	4.123	0.09	17.5	1.35
199.2127143	17.017178	64797 A	6.55	10.9869	0.781	4843	4.47	-0.18	3.3	0.76
216.2991543	51.8507436	70497 A	4.052	14.5307	1.696	6280	4.23	-0.03	28.6	1.33
12.2762275	57.8151773	3821 A	3.444	5.0098	1.068	5907	4.41	-0.28	3.4	1.14
101.5589581	79.5648107	32439 A	5.44	18.2023	1.17	6204	4.43	-0.1	4.5	1.18
222.8460153	19.1019133	72659 B	6.979	6.7486	0.652	4288	4.636	0.144	4.6	0.67

**Table 3** continued on next page

**Table 3** (*continued*)

RA (J2000)	Dec (J2000)	HIP	Vmag	Distance (pc)	Rstar	T <sub>eff</sub>	log(g)	Metallicity	V <sub>sini</sub>	Mstar
302.7997449	-36.1012088	99461 A	5.297	6.0122	0.715	4980	4.62	-0.52	0	0.76
150.252737	31.9236703	49081 A	5.378	14.9263	1.186	5743	4.3	0.2	1.8	1
236.0075774	2.5151668	77052 A	5.869	14.7927	0.942	5682	4.47	0.05	4.1	0.94
52.3444893	-62.9375289	16245 A	4.703	21.7816	1.658	6662	4.31	-0.17	13.1	1.32
76.8625232	18.6450499	23835	4.915	15.9172	1.594	5691	4.06	-0.2	2.36	1.04
258.8365985	-26.6016992	84405 A	5.07	5.9523	0.724	5132	4.53	-0.22	4.3	0.85
173.6228602	-32.8313397	56452 A	5.956	9.559	0.751	5196	4.6	-0.4	0.9	0.88
219.8960963	-60.8375276	71681	1.35	1.3319	0.859	5244	4.54	0.24	3.52	0.94
143.9145925	35.8101325	47080 A	5.402	11.2348	0.969	5518	4.44	0.34	2.3	0.94
133.1492129	28.3308208	43587 A	5.96	12.5868	0.948	5292	4.4	0.32	2.2	0.95
198.5631031	-59.1032372	64583 A	4.913	18.24	1.475	6238	4.23	-0.31	13.8	1.25
24.1993398	41.4054587	7513 A	4.1	13.4916	1.611	6154	4.17	0.08	9	1.18
76.377732	-57.4727047	23693	4.701	11.6927	1.064	6158	4.43	-0.18	12	1.14
214.753732	-25.815425	69965 A	5.872	17.9888	0.978	6120	4.41	-0.68	3.6	1.11
341.6732494	12.1728858	112447 A	4.2	16.1509	1.852	6193	4.07	-0.27	7.7	1.25

**Table 4.** The primary telescope and spectrograph combinations considered. While specific telescopes are listed, these are nominal ones chosen as representative 4/8/12 m class observatories. The collecting area of the 2x8.4 m is simulated as a single 11.78 m telescope.

Telescope	Diameter (m)	Instrument	Wavelength Range (Å)	Nominal Precision (cm/s)
WIYN	3.5	NEID	3800 - 9300	27
LBT	8.4x2	NIRS	9700 - 13000	40
WIYN	3.5	Super NEID	3800 - 9300	3
LBT	8.4x2	Super NEID	3800 - 9300	3
LBT	8.4x2	Super NIRS	9700 - 13000	3

### 3.2. Exposure Time/Precision

In principle, it is possible to figure out exposure times “on the fly”. This is not done due to: the expectation that it would take too long/be too computationally intensive, and that the current atmospheric model does not have a very large effect on precision at high airmass. So a single “good but imperfect” time is used, with assumptions about what that should be.

The aspects of instrumentation considered by Beatty are: wavelength coverage, and the resolution of the spectrograph. This is expanded somewhat in that the telescope and instrument are simulated to the point of basic signal to noise considerations on each pixel, and exposure and readout times.

The readout noise formula is:

$$\frac{\text{photons} \cdot \text{gain}}{\text{pixels} \cdot \sqrt{\text{photons} \cdot \text{gain}/\text{pixels} + (\text{gain} \cdot \text{dnoise} \cdot 2.2 \cdot 2 \cdot \text{exposures})^2 + (\text{gain} \cdot \text{darkcurrent} \cdot \text{exptime})^2}} \quad (1)$$

A generic/other noise term is also included, which describes all unmodeled noise and is treated as an undefined part of an instrument’s noise budget. The generic/other noise is added in quadrature with the (readout) noise to give an overall noise level, which is assumed to be the standard deviation of a Gaussian. A random “measurement” is generated from this overall noise level, and then used for fitting once actual signals have been added in.

### 3.3. Exposure Time Estimation

Exposure time calculation is done via scaling assumptions in the high SNR regime. An initial “guess” is performed by finding the RV precision and SNR at the site when the detector is saturated at whatever wavelength the star is brightest at. To make the guess closer to reality, the signal is attenuated through the airmass at  $10^\circ$  off of zenith, and readout noise is doubled. These seemingly ad-hoc considerations are to consider that the actual exposure is likely to be a co-add of several shorter ones and at more than one airmass. The actual exposure time is then rescaled by a factor of  $\left(\frac{\text{guessRV}}{\text{targetRV}}\right)^2$ . If there is a signal to noise requirement, SNR is rescaled in the same way, and the longer time of it or radial velocity is used.

Times under a minimum are increased to that minimum so as to average out over p-mode oscillations. This is to minimize the effect of this noise source and convert it from correlated to uncorrelated.

In previous work (Newman et al. 2023), we used a fixed 5-minute (and then for comparison a fixed 10-minute) minimum. A more detailed look is appropriate here, as is calculating the actual p-mode timescales using our in-hand stellar properties.

As these times vary per-star, we look at the effects of instituting two fixed (5 minute and 10 minute), and two variable minimum times per star. The first of the variable versions scales with a star's dynamical timescale  $\tau \sim \sqrt{R^3/M}$ , where we define the sun as having a time of 300 seconds:

$$T_{min} = 300 \sqrt{\frac{(R/R_\odot)^3}{M/M_\odot}} \quad (2)$$

This is in contrast with Chaplin et al. (2019) and Luhn et al. (2023), which use surface gravity and effective temperature to find the pulsation frequency:

$$\nu = 3100 \mu Hz \left( \frac{g}{g_\odot} \right)^1 \left( \frac{T_{eff}}{T_{eff,\odot}} \right)^{-0.5} \quad (3)$$

Here,  $g$  is the actual surface gravity, and not  $\log(g)$ .

Our minimum period is then  $\nu^{-1}$ . For the Sun this is 322 s, which is within 10% of the previous scaling. As shown in sections 7,6,8, outside of the short exposure limit, we don't find particularly large differences in results for any p-mode compensation algorithm.

These just generate the “open shutter” time, so the number of exposures to avoid saturating the detector is counted, and the readout times added in to give a total exposure time. We do not impose any upper limit on exposure times, so depending on the input parameters, impractically large ones can be generated. That these stars rarely or never be observed is discussed in section 9, and points to how EPRV target selection must be done with care even in the absence of stellar activity.

#### 3.4. Atmospheric Effects

Our atmospheric absorption/scattering model uses Rayleigh scattering plus a small baseline.

$$\tau = 0.09 + \left( \frac{3080\text{\AA}}{\lambda} \right)^4 \quad (4)$$

This relation was found by fitting measurements from CFHT at Mauna Kea<sup>4</sup>, and Texas A&M University (Schmude 1994). Sky brightness and line absorption are not considered.

The above gives an optical depth at a specific wavelength and 1 airmass. actual absorption considers altitude and zenith angle using simple isothermal (default scale height 8400 m), and slab ( $1/\cos(\theta)$ ) models, respectively.

This is sufficient for ultraviolet, visible, and the nearest infrared wavelengths, but breaks down once water absorption starts to matter (approximately 890 nm). Expanding into this range would be preferable, but would require line-by-line analysis instead of the current continuum model. This is a consideration for future work, but would significantly increase complexity.

Beyond reducing the strength of RV information, line-based absorption also introduces uncertainties which are not modeled here. Scattered/absorbed light is assumed to simply be lost, and any errors in

<sup>4</sup> <https://www.gemini.edu/sciops/telescopes-and-sites/observing-condition-constraints/extinction>

242 lines from microtellurics are assumed to be perfectly modeled. We partially account for microtelluric  
243 errors with nominal noise values in section 6.4.

244 Clouds/hazes are not considered (beyond the wavelength-independent portion of the absorption  
245 acting as particulates), nor does the model include weather or season variations in sky quality. A  
246 night is assumed to be perfectly clear, or unusable/no observations are possible.

### 247 3.5. Stellar Activity

248 We do not directly model any form of stellar activity (eg: oscillations, granulation, spots/plages).  
249 Indirectly, we both choose a target list to contain relatively inactive stars (eg: low  $R_{HK}$  values),  
250 and our exposure times compensate for p-mode oscillations (see 3.3). We expect that observation  
251 campaigns with high cadence and a large number of observations can better model activity to reduce  
252 “jitter”, but this lack of direct modeling can lead to our expected sensitivities and SNRs being  
253 optimistic by a factor of several.

254 In contrast, Luhn et al. (2023) which models stellar variability with 4 terms: 1 for activity, 1 for  
255 oscillation, and 2 for granulation. The active regions use a solar-specific model, while oscillations  
256 and granulations consider spectral type. Our p-mode calculations herein substantially addresses the  
257 oscillation portion of the noise, as we look at: Luhn’s timescales, an alternate timescale that also  
258 scales with spectral type, and 2 fixed ones. Additional strategies are needed for the other forms  
259 of stellar variability. Both more realistic active regions, and observing strategies to mitigate active  
260 regions and granulation are deferred for future work.

261                  4. DISPATCH SCHEDULER (SURVEY SIMULATIONS)

262        The dispatch scheduler simulates an observational campaign to generate observation time series  
 263        for later use. Our version<sup>5</sup> is derived from the MINERVA scheduler (Swift et al. 2015; Nava et al.  
 264        2015). The scheduler takes a list of targets with name, RA, Dec, and observation times as inputs,  
 265        and generates a time series of observations for each target (as well as the Sun and each target’s  
 266        rise and set times). It also generates a nightly summary file containing: start and end of the night,  
 267        weather, number of times each star was observed, amount of time spent on each star, and if the  
 268        star was observable at all given our constraints. Constraints define the ordering and prioritization  
 269        of targets to observe. These observation constraints can be divided into: natural, observatory, and  
 270        prioritization weights.

271        For natural constraints, we consider: latitude, longitude, local weather (fraction of clear nights),  
 272        target acquisition, elevation, and local horizon. Calculated sun-rise/set times are used, and a mini-  
 273        mum distance from the Moon is specified (ephemeris via Astropy). For the observatory constraints,  
 274        we consider local horizon, acquisition/repointing time, and observation/readout time.

275        As per the name, we use a dispatch scheduler prioritization scheme. The scheduler determines  
 276        target choices “on the fly”, and we consider several different prioritization weighting options that we  
 277        discuss in Section 4.1.

278        A typical night works as follows:

- 279        • Advance time to “full dark” (configurable, by default astronomical twilight, where the sun is  
 280        12 degrees below the horizon)
- 281        • Check to see if the night is clear, or lost due to weather
- 282        • If the night is cloudy, advance time to dawn
- 283        • If the night is clear, prep target list (determining which stars are observable due to sufficient  
 284        separation from the moon, and being above the horizon)
- 285        • Begin observation loop

286        Observation loop:

- 287        • Generate weightings for the target stars
- 288        • Pick highest weighted target
- 289        • If the target has a positive weight, observe it for the duration specified
- 290        • Wait five minutes (this is done whether or not a target is observed.)
- 291        • Repeat until dawn

292        Observations are recorded as they are taken. If no target has a positive weight, this means that  
 293        no observations are taken with the telescope, and we record the telescope downtime separately. At  
 294        dawn, we record the Sun and target rise and set times, a nightly summary of target observations  
 295        observability and weather, and move to the next night. Dawn can be specified to mean that the sun

<sup>5</sup> Available at [https://github.com/pdn4kd/dispatch\\_scheduler](https://github.com/pdn4kd/dispatch_scheduler)

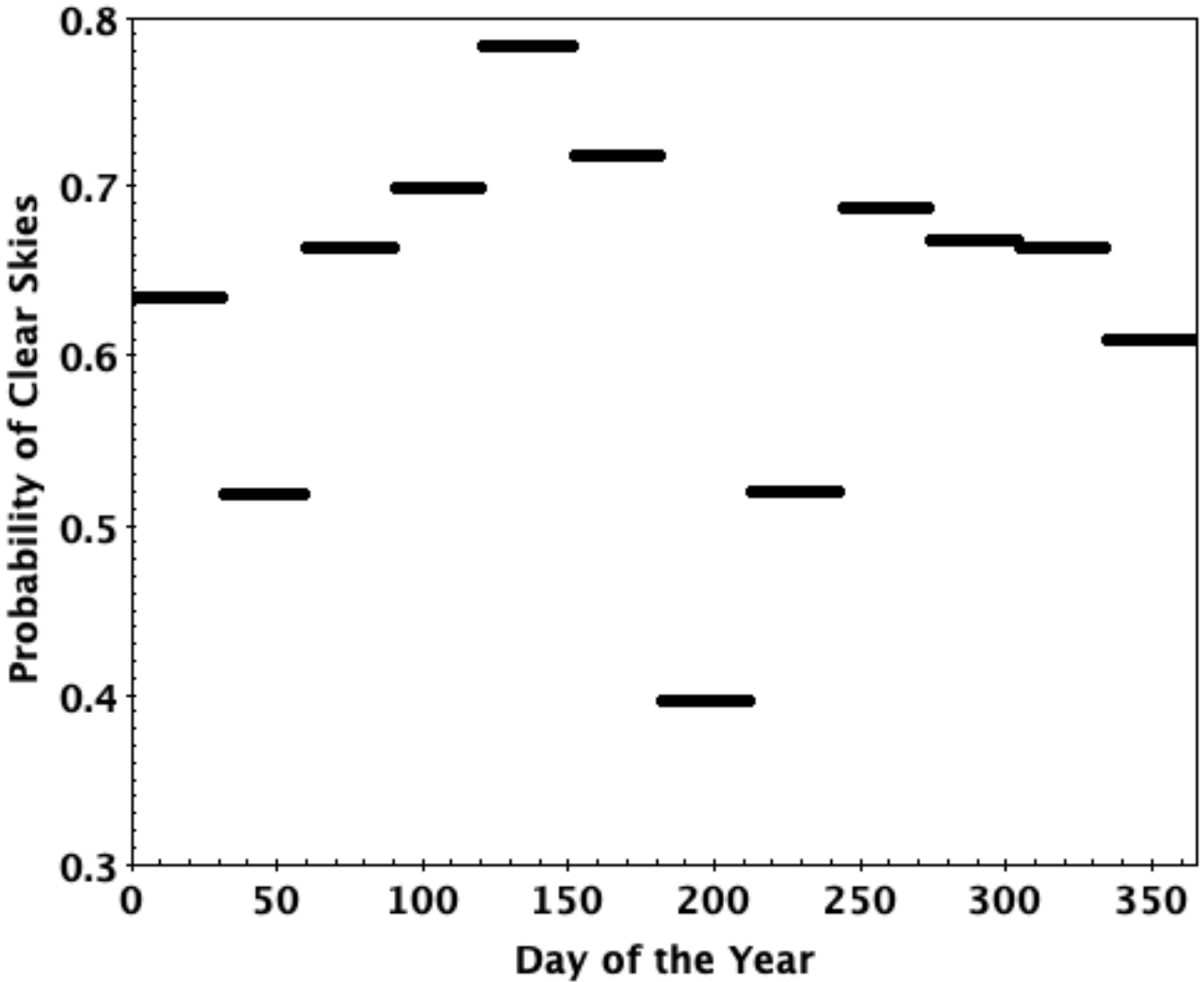


**Figure 1.** Monthly WIYN observing and weather statistics from 1999 to 2006. Adapted from [http://www-kpno.kpno.noao.edu/Images/wiynWeather\\_stats.jpeg](http://www-kpno.kpno.noao.edu/Images/wiynWeather_stats.jpeg)

is still below the horizon, depending on what settings are specified. Days/nights will alternate until the observation campaign is completed.

Finally, we assume that 100% of telescope time is available for a RV survey. Treating the weather as worse/lower probability of a clear night can effectively simulate random queuing without affecting the weighting system. Implementing bright/dark time scheduling would be a subject for future work, as the exact definition varies between observatories.

#### 4.1. Target Weighting

As we do not plan our observations in advance, we need to figure out which star to observe multiple times per night. Our weighting constraints were chosen to maximize the total number of observations while minimizing the variance between stars. More observations are of obvious value, but we also expect that higher planet yields will be best served by relatively even survey depth. To achieve

307 these, we focused on weighting schemes using hour angle/meridian distance, as well as time since last  
308 observation.

309 Hour angle weighting is an attempt to maximize observation quality without penalizing stars at  
310 unfavorable declinations. It varies linearly from 1 at the meridian to 0 at the horizon. The time since  
311 last observation weighting is the number of days since last observation after the minimum separation  
312 between observations has passed. Before this it is set to 0. Regardless of other considerations,  
313 “unobservable” stars are assigned a weight of -999. Observable is defined as: above the nominal  
314 horizon for the duration of the observation, sufficiently far from the moon (10 degrees by default),  
315 and that the observation will finish before sunrise.

316 After iterating through different versions of these weightings (see section 9.4), we settled on using  
317 hour angle multiplied with time since last observation, with a minimum time of 2 hours. These  
318 combined weighting will in practice prioritize stars that have not been observed in a given night that  
319 are anywhere within a telescope’s pointing limits over ones that have at the zenith.

## 5. RESULTS (OVERVIEW)

In this section, we discuss the overall outline of the results, and what we look at in terms of outcomes. First we introduce figure of merit we use for detection efficiency (section 5.1), which along with exposure times and numbers of observations, we will use for all subsequent simulations that are not directly testing the survey simulation code. We then show a few example outputs before proceeding with the results of different target lists and simulation parameters:

We show example timeseries results in in Figure 2, before going into general target list results.

We primarily focus on the HWO target list. All results are for a surface gravity/effective temperature p-mode timescale and hour angle with 2 hour minimum observation separation target weighting. For this we show: exposure times, observations, and how those correlate; exposure times as a function of selected stellar parameters; observations as a function of selected stellar parameters. We show our detection heuristic/figure of merit in some plots, as well as how those detections are degraded by uncorrected telluric effects.

Detailed reasons for why we choose a specific p-mode compensation method and target weighting are described in 9.4.

The EPRV and HabEx target lists are then covered briefly, with more of their differences and how target list selection changes results in 9.6.

### 5.1. Figure of merit: planet semi-amplitude sensitivity and detection SNR

Herein, we use a figure of merit for detecting a plausible planet with some simplifying assumptions: For an uninformed survey where the period observed is much longer than than the planet, the planet's orbit is circular and edge-on, and the distribution of observations is random/planet phase is unknown (Gaudi & Winn 2007):

$$SNR = \frac{K}{\sigma} \sqrt{\frac{N_{obs}}{2}} \quad (5)$$

$$K = SNR \cdot \sigma \sqrt{\frac{2}{N_{obs}}} \quad (6)$$

The noise term,  $\sigma$ , can be broken down into multiple noise sources added in quadrature (photon, instrument, tellurics, etc). eg:

$$SNR = \frac{K}{\sqrt{2}} \sqrt{\frac{N_{obs}}{\sigma_{instrument}^2 + \sigma_{photon}^2 + \sigma_{atmosphere}^2}} \quad (7)$$

$$K = SNR \cdot \sqrt{(\sigma_{instrument}^2 + \sigma_{photon}^2 + \sigma_{atmosphere}^2) \frac{2}{N_{obs}}} \quad (8)$$

For analysis in this paper, we use equations 7 and 8, with the atmospheric noise term being zero in all sections except for the telluric noise ones.

### 5.2. Example Timeseries

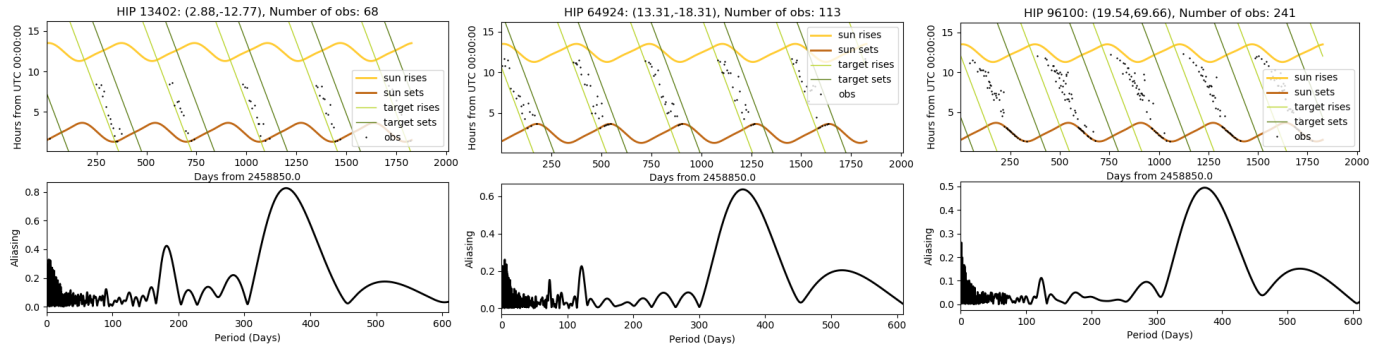


**Figure 2.** Example survey results from a 5 years/100% time with Super NEID (3 cm/s) on the WIYN. The top graph shows target rise and set times, sunrise and sunset times, and target observations over the course of the survey. The bottom graph shows potential aliasing/false planet signals from the distribution of observations over various orbital periods. Patterns in observations as a result of long exposure times and changing weighting are visible, as well sensitivity limitations for some planets.

## 6. RESULTS (HWO TARGET LIST)

### 6.1. Exposure Times and Observations

351

352

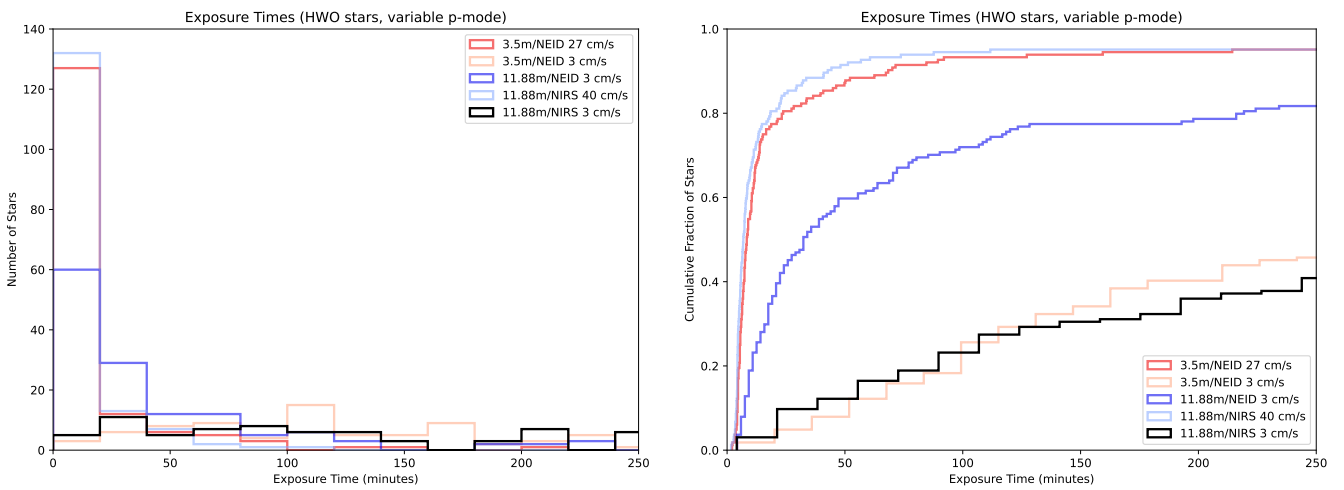


**Figure 3.** Exposure times as histograms (left) and cumulative distribution functions (right) for every star in our telescope/instrument combinations. There is a tail of stars with very long exposure times (and which are therefore difficult to observe at high precision). The PDF appears the same for all 3 sets of stars due to the current bin size of 20 minutes, as whatever chosen p-mode correction has little effect beyond that. Due to finer bin sizes, the CDFs do show that the exact distribution of exposure times is shuffled around somewhat, though the effect is again small (and largely confined to telescope/instrument/precision combinations that skew to shorter exposure times).

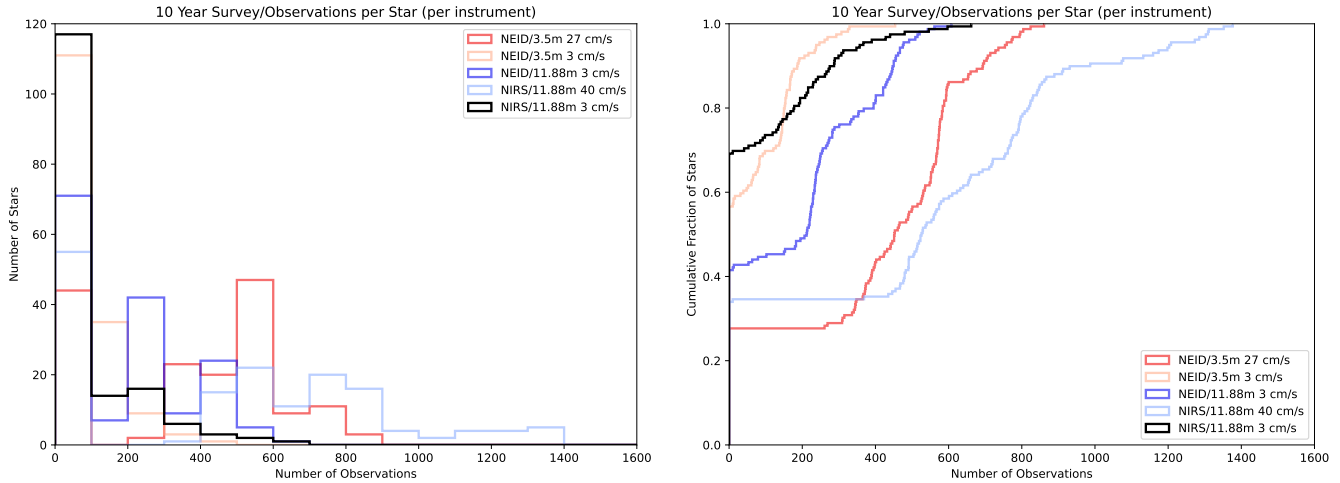


**Figure 4.** Histograms of total number of observations for the different telescope/instrument combinations as both PDFs (left) and CDFs (right). Differences between different architectures are quite obvious, though the ones between different p-mode compensation methods are subtle (and not apparent for the architectures with longer exposure times and fewer observations).

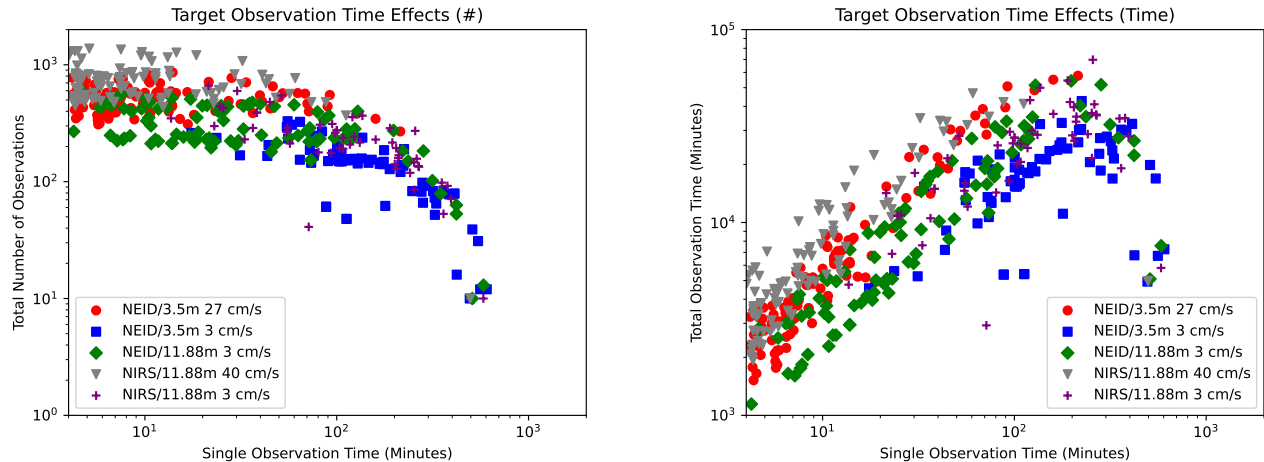


**Figure 5.** Total number of observations (left) and total time spent observing (right) for each star and telescope/instrument combination as a function of exposure time.

## 6.2. Exposure Times and Stellar Parameters

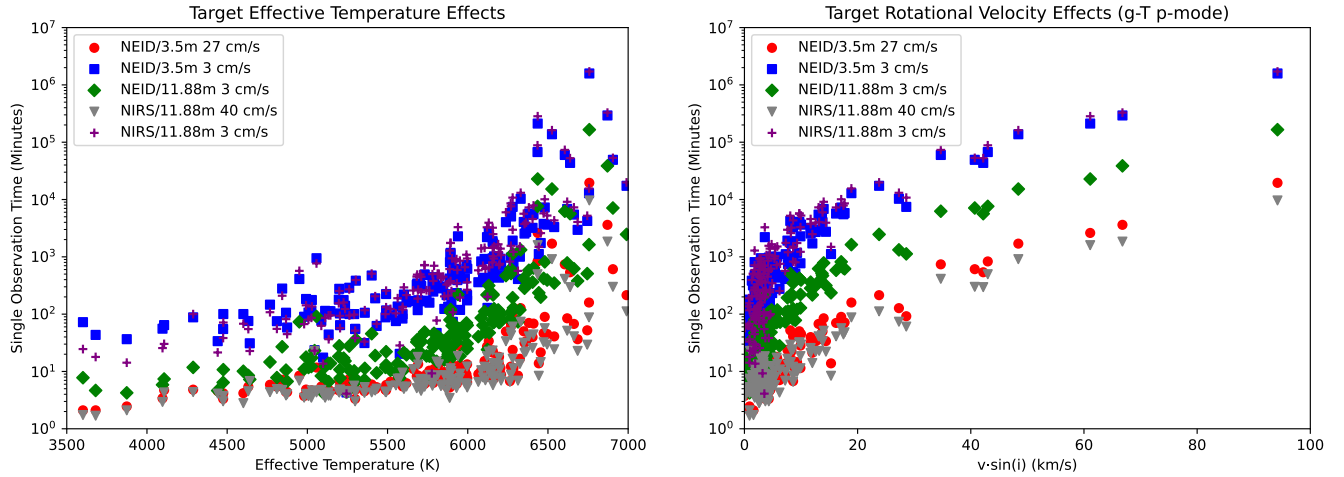


**Figure 6.** Exposure times as a function of effective temperature (left), and rotational velocity (right), for the gravity/effective temperature P-mode compensation. While we see clear trends of hotter/faster rotating stars being harder to observe, the choice of telescope/instrument/precision usually has a larger effect.

354

### 6.3. Right Ascension and Declination

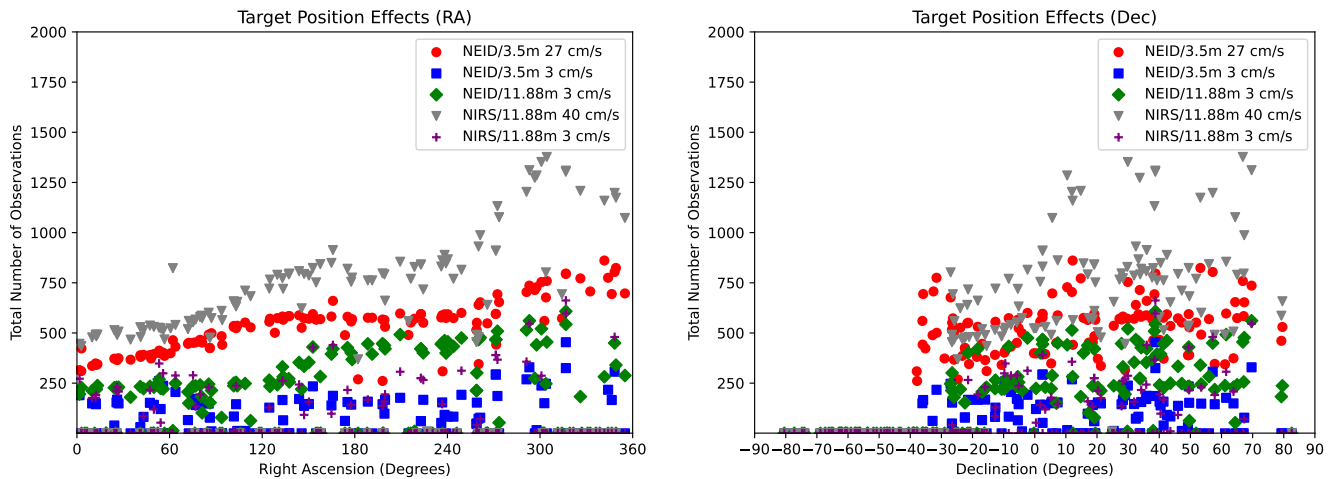


**Figure 7.** Total number of observations per star as a function of Right Ascension (left) and Declination (right). There is a clear trend in right ascension, we believe from a combination of night length and weather (though it is suppressed for longer exposure time telescope/instrument/precision combinations). That the larger peak corresponds with stars that have the longest time above the horizon in late summer (around 300-330 degrees) and not winter/early spring (when the weather is better and nights longer) is surprising. Declination does not show a clear trend, with number of observations per star being relatively flat north of about -40 degrees. Below that, stars are never observed.

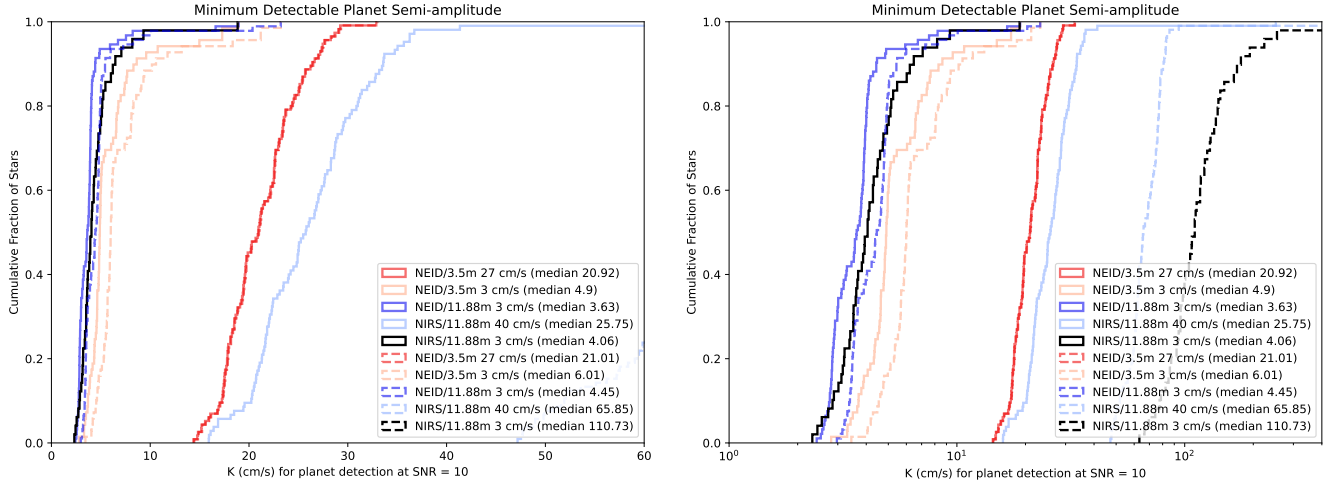


**Figure 8.** CDFs of minimum detectable reflex velocity ( $K$ , in cm/s) of a planet at  $\text{SNR} = 10$  over our telescope/instrument combinations at multiple scales. The results with no microtellurics are shown as solid lines, while the telluric noise are the dotted lines.

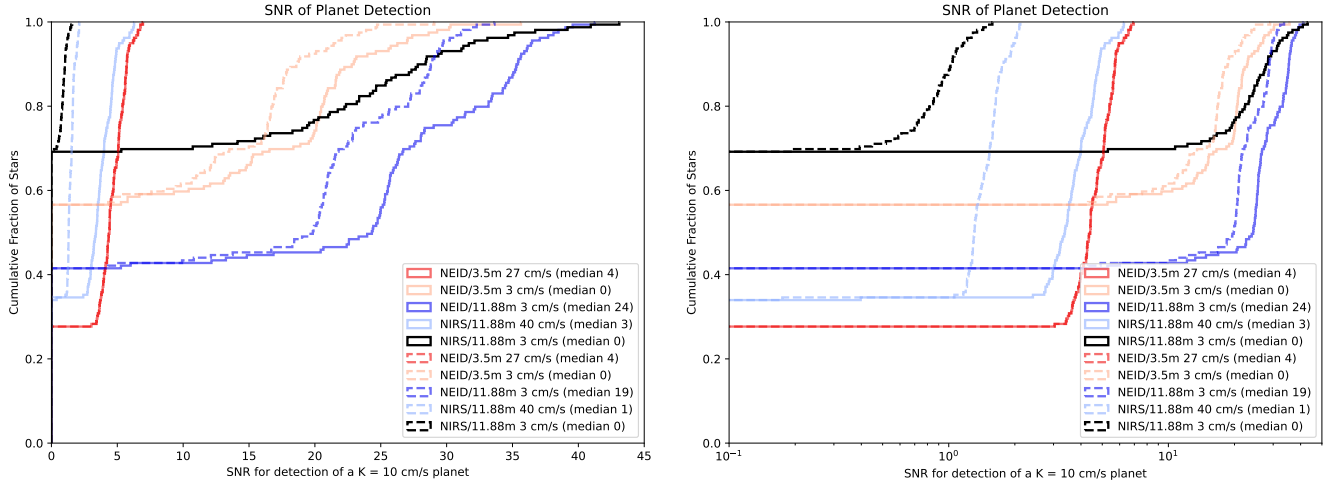


**Figure 9.** CDFs of minimum detectable reflex velocity ( $K$ , in cm/s) of a planet at  $\text{SNR} = 10$  over our telescope/instrument combinations at multiple scales. The results with no microtellurics are shown as solid lines, while the telluric noise are the dotted lines.

#### 6.4. Telluric Corrections

Despite our earlier atmospheric assumptions, earth's atmosphere has many shallow lines that are difficult to correct for, especially in the infrared. To simulate this, we consider an additional noise term added in quadrature with the instrument and photon noise ones. We choose values of 3 cm/s for the visible spectrograph and 115 cm/s for the NIR spectrograph, which are in line with existing EPRV systems. (Wang et al. 2022)

As our assumed noise is smaller than the instrument and photon noise sources in all but the most optimistic visible surveys, microtellurics have little effect. In contrast, this noise source dominates over all others in the NIR (being far larger than the instrument or photon components, even in the

364 most pessimistic cases), and must be better accounted for if this wavelength range is to be useful in  
 365 the EPRV era.

## 366 7. RESULTS (HABEX TARGET LIST)

367 While a full set of simulations were done, for brevity we only post the most relevant ones, using  
 368 the g-T p-mode compensation. We do not go over the results in particular detail, though some of  
 369 the differences are discussed in section 9.

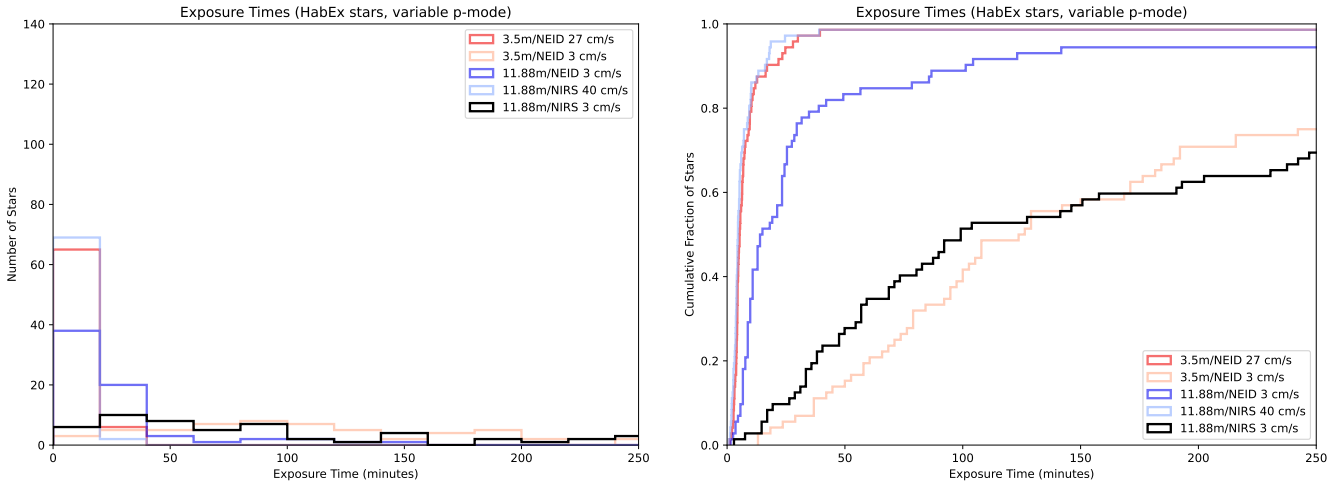


**Figure 10.** Exposure times as histograms (left) and cumulative distribution functions (right) for every star in our telescope/instrument combinations. There is a tail of stars with very long exposure times (and which are therefore difficult to observe at high precision). The PDF appears the same for all 3 sets of stars due to the current bin size of 20 minutes, as whatever chosen p-mode correction has little effect beyond that. Due to finer bin sizes, the CDFs do show that the exact distribution of exposure times is shuffled around somewhat, though the effect is again small (and largely confined to telescope/instrument/precision combinations that skew to shorter exposure times). In all cases, there is a “tail” of stars that have relatively long exposure times, even for favorable telescope/instrument/precision combinations. For less favorable ones, this “tail” can mean that around half of all stars have exposure times of over two hours (and so are difficult to observe).

370 The distributions of observations are largely similar between different p-mode compensation methods,  
 371 with the exception of the fixed 10-minute case for otherwise short exposure times (NEID, 3.5  
 372 m, 27 cm/s and NIRS, 11.88 m, 40 cm/s). For those two telescope/instrument/precision combinations,  
 373 a long fixed p-mode timescale increases the exposure times for most of the stars, and causes a  
 374 noticeable reduction in the number of observations.

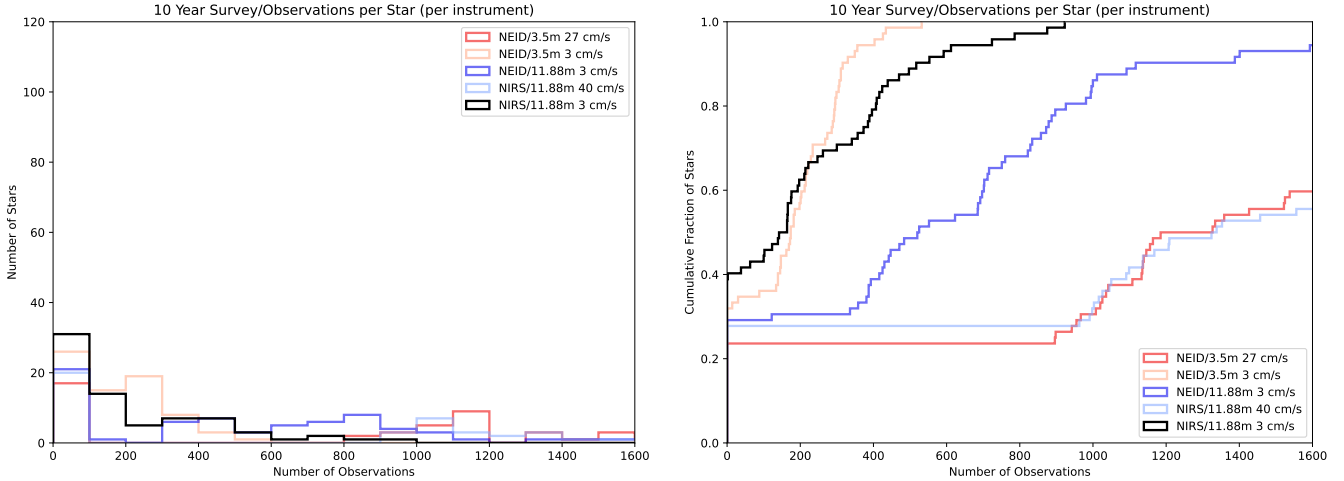


**Figure 11.** Histograms of total number of observations for the different telescope/instrument combinations as both PDFs (left) and CDFs (right). Differences between different architectures are quite obvious, though the ones between different p-mode compensation methods are subtle (and not apparent for the architectures with longer exposure times and fewer observations). Because of the details of the target list (both position and exposure times), between around 25 and 40% percent of the target stars are never observed.

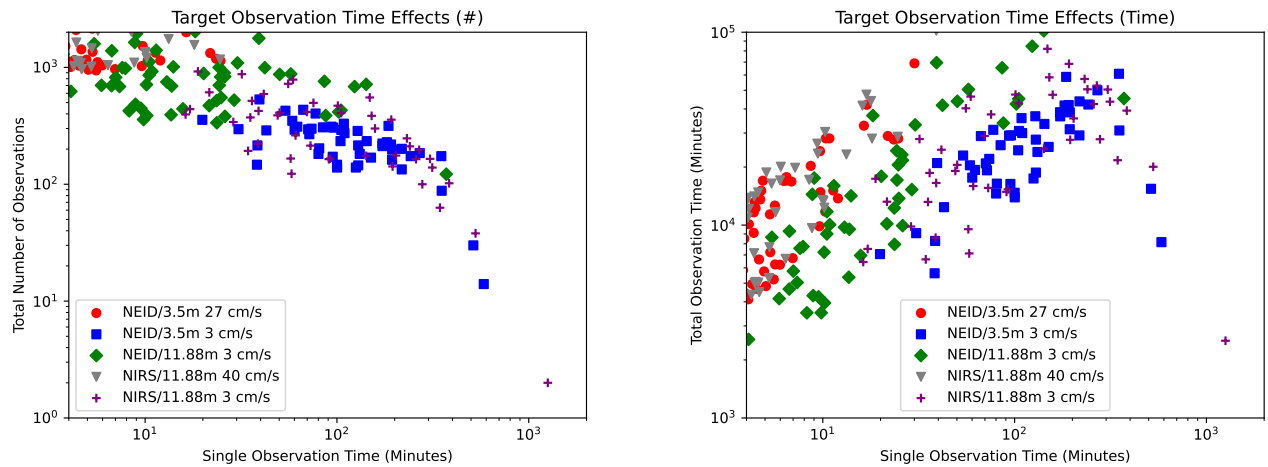


**Figure 12.** Total number of observations (left) and total time spent observing (right) for each star and telescope/instrument combination as a function of exposure time. Number of observations decrease slowly with increasing exposure time (while time spent on a given star increases) until around 300 minutes, and which point both rapidly decrease as the stars become increasingly impractical to observe.

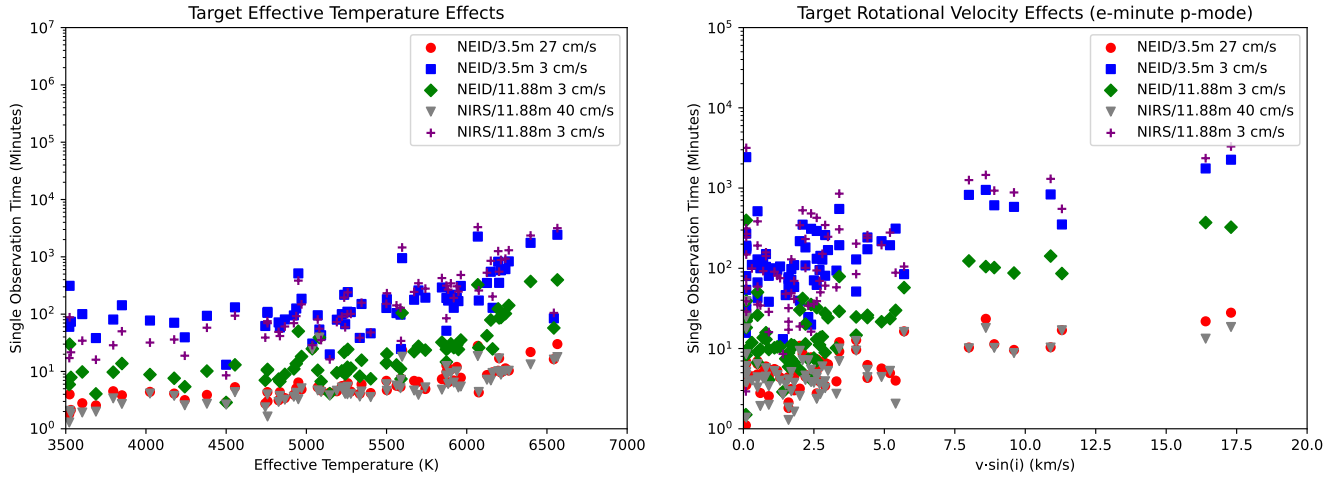


**Figure 13.** Exposure time as a function of effective temperature (left), and rotational velocity (right). This target list shows a clear trend of increasing observation difficulty for hotter stars, though choice of telescope, instrument, and target precision are more important for GKM stars. One star (Altair), is off the top-right corner of the  $v\sin(i)$  plot, due to its unphysically long exposure times at our desired precisions and having a rotational velocity of 211 km/s.

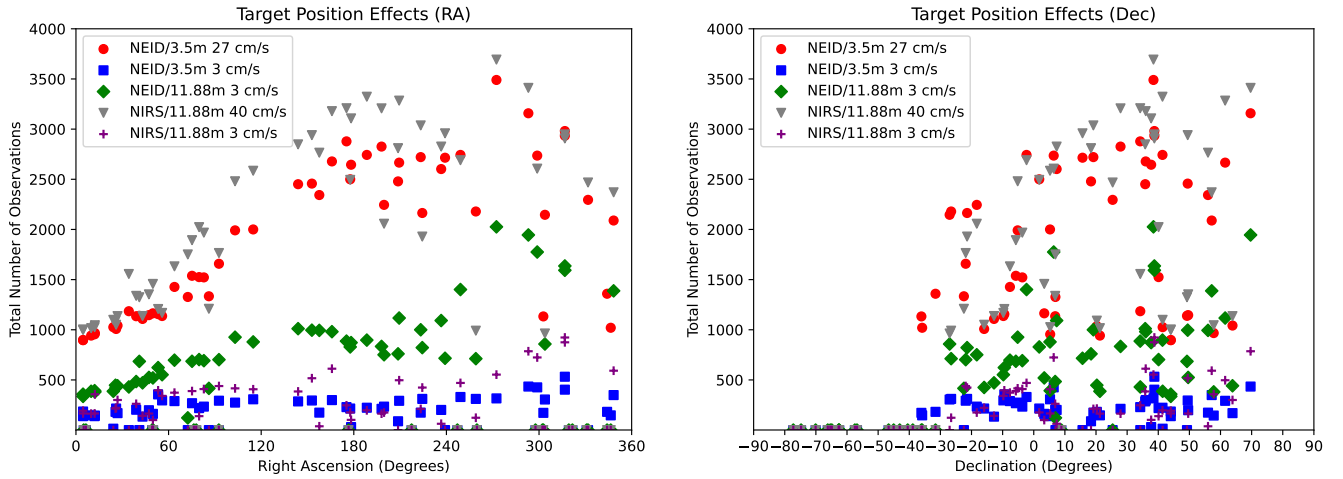


**Figure 14.** Total number of observations per star as a function of Right Ascension (top) and Declination (bottom). There is a clear trend in right ascension, we believe from a combination of night length and weather (though it is suppressed for longer exposure time telescope/instrument/precision combinations). That the peak corresponds with stars that have the longest time above the horizon in late summer (around 300-330 degrees) and not winter or early spring (when the weather is better and nights longer) is surprising. Declination does not show a clear trend, with number of observations per star being relatively flat north of about -40 degrees. Below that, stars are never observed.

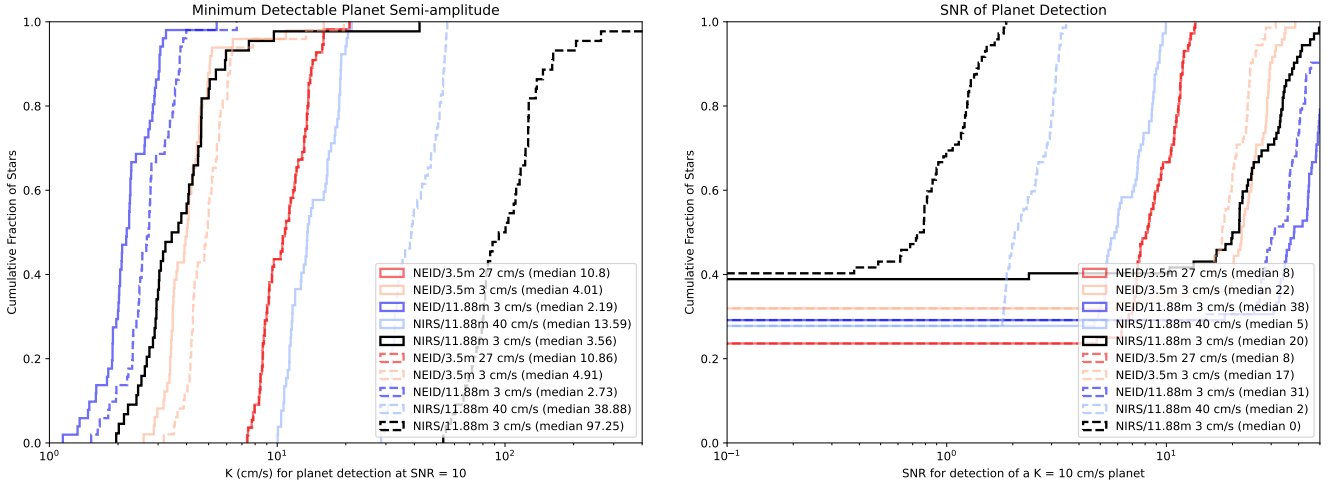


**Figure 15.** How our detection heuristic changes from no microtellurics (solid lines) to nominal microtelluric noise (dotted lines). **Left:** CDFs for the minimum detectable reflex velocity ( $K$ , in cm/s) for a planet at  $\text{SNR} = 10$ . **Right:** CDFs for the SNR for a detection of a  $K = 10$  cm/s planet.

As our assumed noise is smaller than the instrument and photon noise sources in all but the most optimistic visible surveys, microtellurics have little effect. In contrast, this noise source dominates over all others in the NIR (being far larger than the instrument or photon components, even in the most pessimistic cases), and must be better accounted for if this wavelength range is to be useful in the EPRV era.

375  
376  
377  
378  
379

380                   8. RESULTS (EPRV TARGET LIST)

381       To avoid redundancy, only the results using the surface gravity/effective temperature variable p-  
382       mode correction are shown.

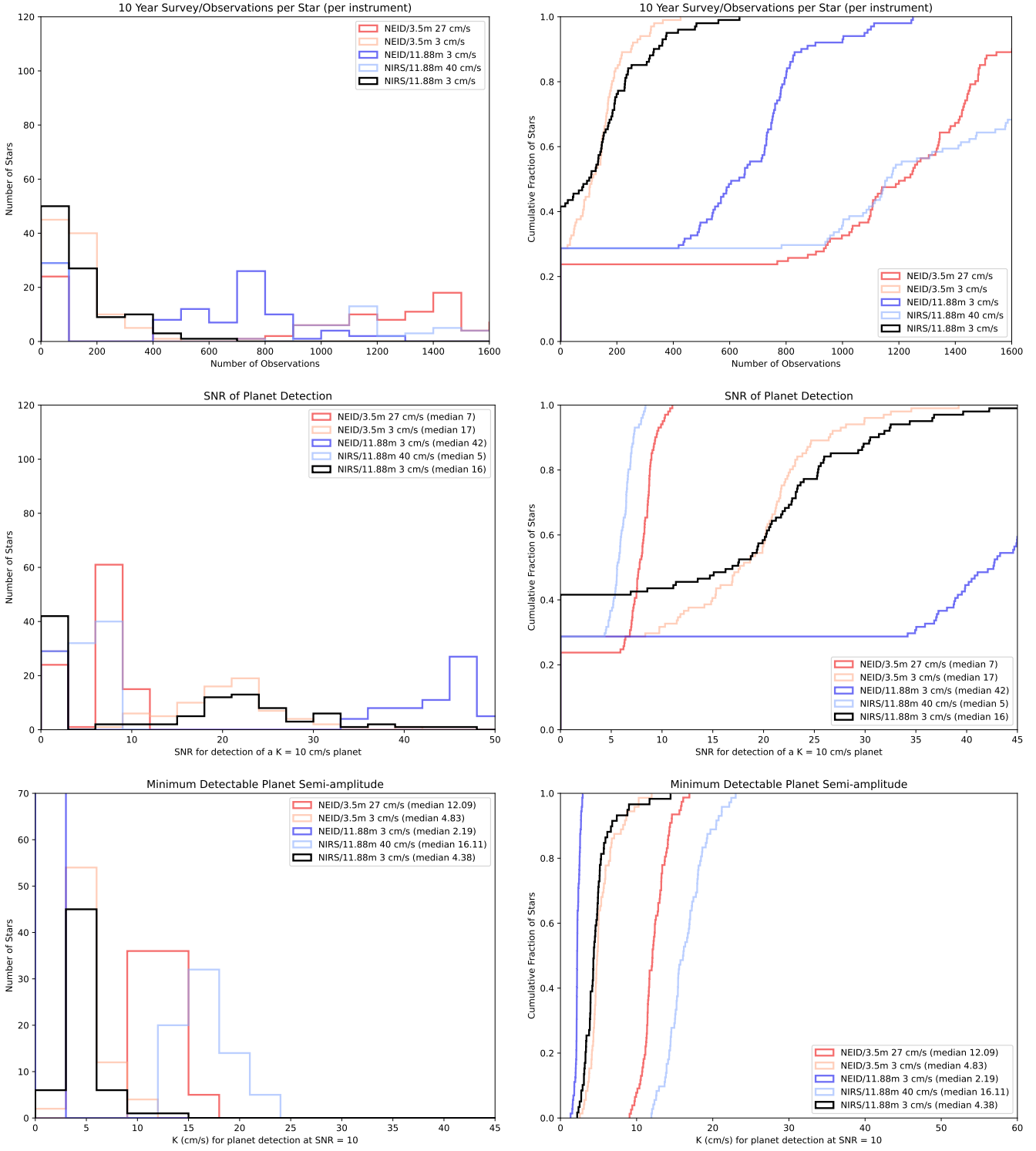


**Figure 16.** Histograms/PDFs (left) and CDFs (right) of the number of observations (top), SNR of a nominal  $10 \text{ cm/s}$  planet detection (middle), and minimum detectable reflex velocity  $k$  of a nominal  $\text{SNR} = 10$  planet detection (bottom).

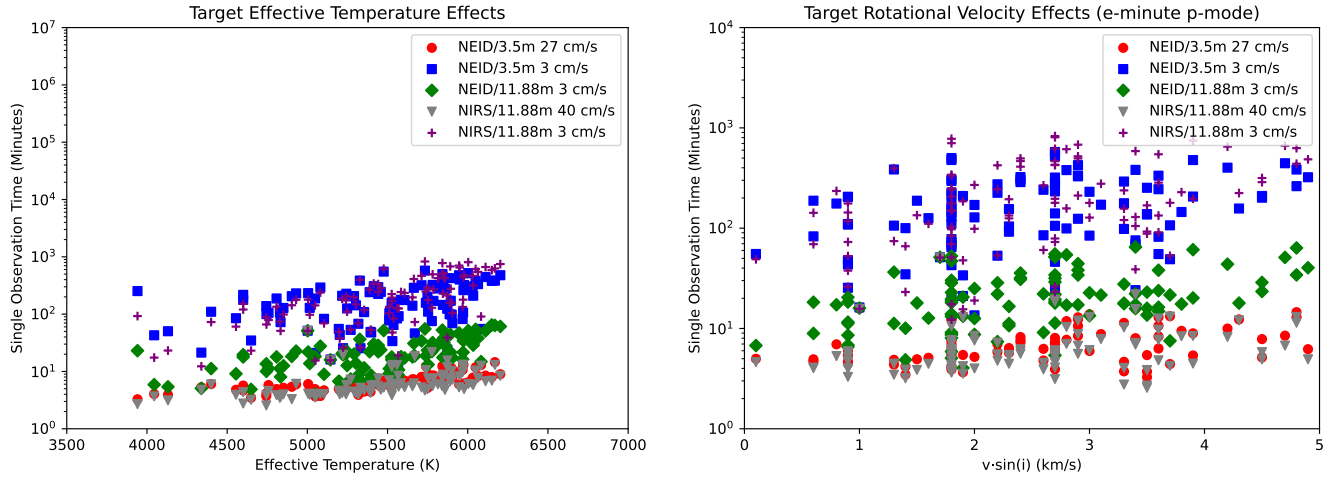


**Figure 17.** Exposure time as a function of effective temperature (left), and rotational velocity (right). This target list shows a clear trend of increasing observation difficulty for hotter stars, though choice of telescope, instrument, and target precision are more important for GKM stars. There is no clear trend in exposure time for  $v\text{-} \sin(i)$ , possible due to all stars in this sample being slow rotators.

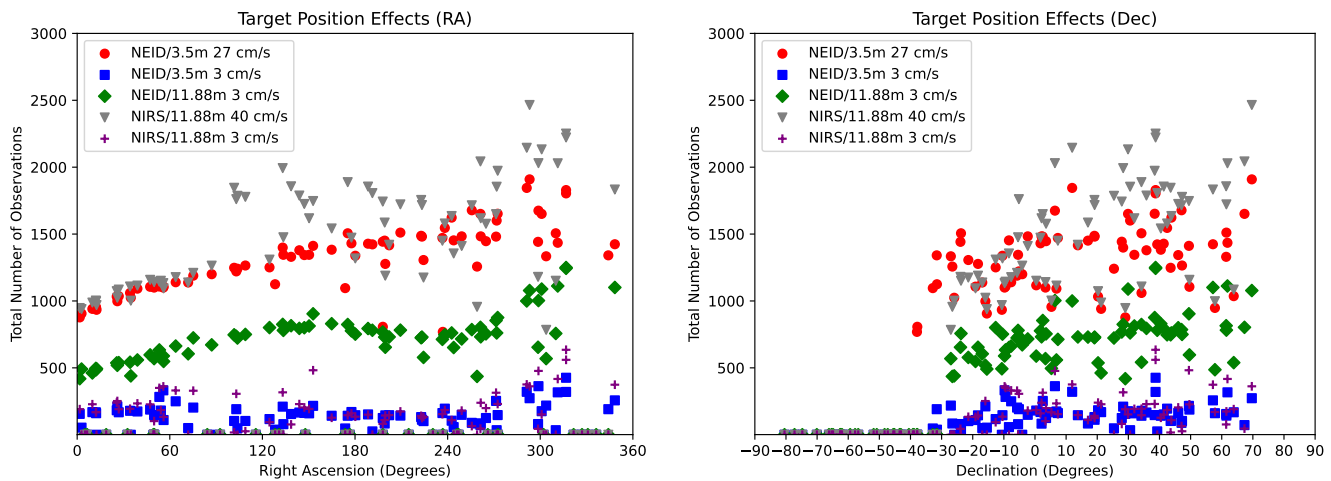


**Figure 18.** Total number of observations per star as a function of Right Ascension (left) and Declination (right). There is a clear trend in right ascension, we believe from a combination of night length and weather (though it is suppressed for longer exposure time telescope/instrument/precision combinations). That the peak corresponds with stars that have the longest time above the horizon in late summer (300-330 degrees) and not winter/early spring (when the weather is better and nights longer) is surprising. Declination does not show a clear trend, with number of observations per star being relatively flat north of about -40 degrees. Below that, stars are never observed.

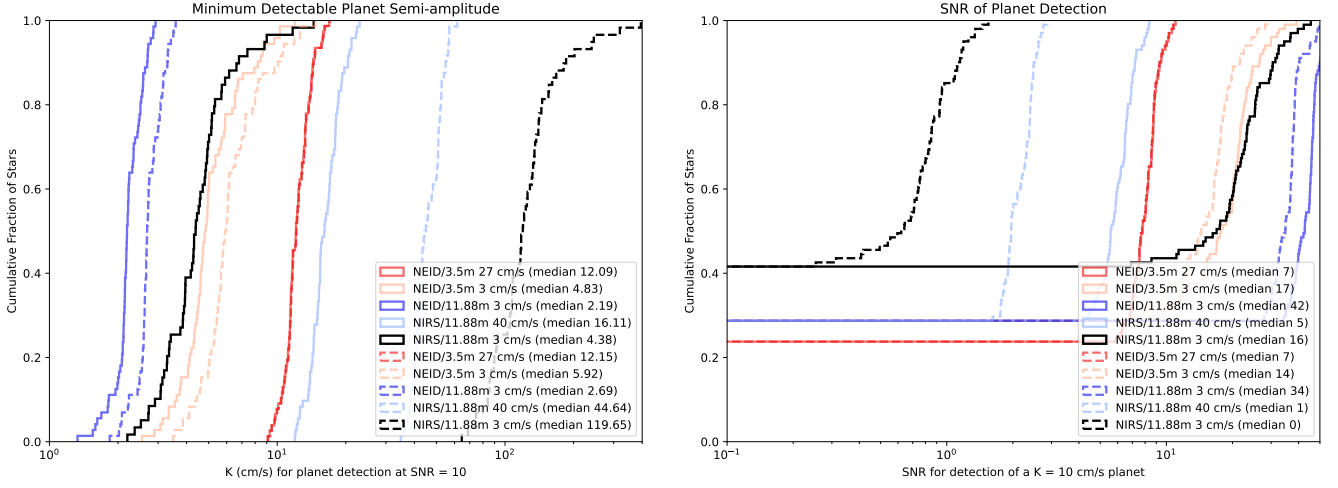


**Figure 19.** How our detection heuristic changes from no microtellurics (solid lines) to nominal microtelluric noise (dotted lines). **Left:** CDFs for the minimum detectable reflex velocity ( $K$ , in cm/s) for a planet at  $\text{SNR} = 10$ . **Right:** CDFs for the SNR for a detection of a  $K = 10$  cm/s planet.

383 As our assumed noise is smaller than the instrument and photon noise sources in all but the most  
384 optimistic visible surveys, microtellurics have little effect. In contrast, this noise source dominates  
385 over all others in the NIR (being far larger than the instrument or photon components, even in the  
386 most pessimistic cases), and must be better accounted for if this wavelength range is to be useful in  
387 the EPRV era.

388

## 9. DISCUSSION

389

### 9.1. Exposure Time Considerations

390

Exposure time is an incomplete proxy for ease of observations, with other factors (discussed below) also being relevant. Difficult targets receive fewer exposures, though total time allocated to observing them only falls off when they become almost unobservable. The boundary between difficult and impossible to observe can be fuzzy for actual observations (until one reaches exposure times that are unphysically long), so our exposure time calculator makes no attempt to distinguish these.

391

Our exposure time calculator can, depending on inputs, generate arbitrarily long exposure times. We do not consider this a problem because: there is no clear cutoff for what makes a star impractical to observe, and the relative times are still useful as figures of merit. Depending on the survey goals, it is possible that they will want to: accept lower precision, tolerate long exposures, or drop the target entirely. We did not impose any limits on what times we accept in our simulations because we both wanted to get a feel for what was impractical within our assumptions, and our code gracefully deals with lists containing unobservable targets.

402

### 9.2. Comparisons to Other Exposure Time Calculators

403

Herein we compare our ETC considerations and results with some that are used for planning purposes at actual observatories, including one with one of our nominal instruments. As these sorts of ETCs are for planning out approximate time allocation needed, we expect that while results will approximately correlate, they will not be exact. Different systems are optimised for different types of targets, depending on typical observatory usage. Additional features that are subjects of ongoing research (eg: stellar activity) cannot be a-priori described to high detail because we do not yet know them in high detail.

410

#### 9.2.1. ESPRESSO ETC

411

ESPRESSO is an existing EPRV instrument on the VLT at Paranal. Its exposure time calculator (Boffin et al. 2024) is available on the web<sup>6</sup>, and herein we compare the results.

412

This ETC has a large variety of spectral models, though there is a focus on giant stars and non-blackbody emission. For stars, they use a grid of atmospheric models, with options for their instruments, differing sky conditions, and single vs four telescope observing programs. The calculator is somewhat more focused on faint/low surface brightness (eg: extragalactic) sources, with the inclusion of sky brightness, with limited options in terms of sun-like stars. Though like us they gloss over line effects in the IR. It is well designed for planning with individual targets and specific dates, though the web interface would be a hassle for preparing for a large survey.

420

For the purposes of trends across spectra type, we look at exposures for a limited subset of stars:

Spectra Type	S/N	RV precision (m/s)
G0	151.882	0.4
G2V	152.606	0.39
K2V	153.587	0.39
K7V	155.971	0.38
M2V	150.353	0.4

<sup>6</sup> <https://www.eso.org/observing/etc/bin/gen/form?INS.NAME=ESPRESSO+INS.MODE=spectro>

422 There is a similar pattern (at least for constant V-mag) of getting consistent RV precision for a  
 423 given exposure time across a fairly wide spectra type range. Using their most optimistic Precipitable  
 424 Water Vapor, seeing, and Moon illumination figures and at the same airmass as we did.  
 425

We do not perform other comparisons, given the differences in what our ETCs focus on.

#### 426 9.2.2. NEID ETC

427 NEID's ETC is available both in web interface and downloadable forms<sup>7</sup> for observation planning.  
 428 It is more tightly focused on stellar RVs (in-line with the telescope/instrument's tighter focus). They  
 429 use a pre-computed grid of stellar models at various effective temperatures, and return precision based  
 430 on that effective temperature and v-mag. Importantly, they reject any target/precision combination  
 431 that would have a single observation time longer than 3600 seconds, so our comparisons focus on the  
 432 lower precision/shorter exposure time end. We specifically look at both synthetic stars for overall  
 433 trends (9.2.2), and a direct comparison of our target lists (9.2.2).

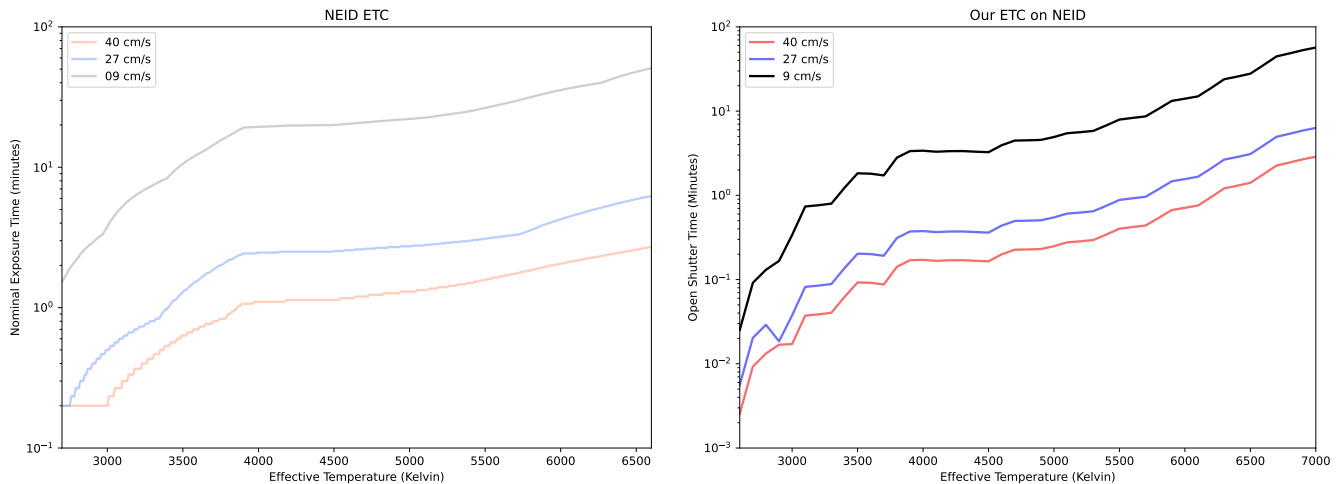


**Figure 20.** **Left:** Nominal exposure times at 3 RV precisions on NEID for synthetic stars that have an apparent V-magnitude of 4.83 as a function of effective temperature (so an unrealistic approximately constant luminosity, thus showing RV information content for a more or less constant number of photons as a function of temperature). The values are calculated with NEID's official ETC over their modeled range (2700 to 6300 K). Lower values are "better" (higher precision). **Right:** Equivalent synthetic stars stars (apparent magnitude 4.83, constant vsini, metallicity, and log(g), but with varying effective temperature) with exposure times calculated by our ETC. Both show similar trends, though the exact times are offset from each-other by about an order of magnitude. Given that none of these stars are especially real, such an offset is not concerning.

434 Our ETC approximately agrees with NEID's, though there are significant differences in details,  
 435 potentially resulting in a factor of several longer or shorter exposure time. We believe that this is from  
 436 our considering additional stellar parameters, while also using comparatively simplified atmospheric  
 437 and instrumental parameters. Given that the spread of exposure times overlap and our surveys all  
 438 use target lists with a range of exposure times, these differences do not constitute a problem for

<sup>7</sup> [https://bitbucket.org/erik\\_timmermann\\_noao/neid-etc/src/master/](https://bitbucket.org/erik_timmermann_noao/neid-etc/src/master/)

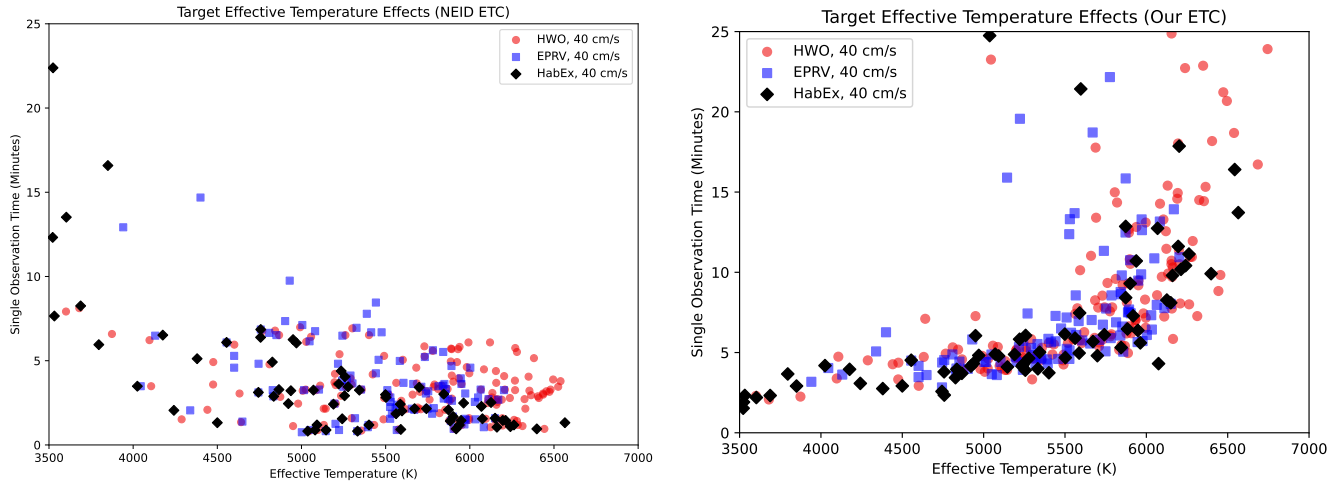


**Figure 21.** **Left:** Exposure times for the stars in our 3 target lists for a nominal single exposure at 40 cm/s, using the NEID ETC. Stars with exposure times longer than one hour are not shown. Depending on the target list, there can be a trend towards shorter exposures for hotter stars, but this is not always the case and it is relatively flat for stars hotter than around 4500–5000 K. If one wanted to choose a target list with a specific exposure time cutoff, they could do so while having stars across a broad temperature range. **Right:** The same target lists at the same scale are shown with our own exposure calculator. The higher “floor” in our times is from our p-mode compensation, and the upwards scatter at high temperatures is from increased  $v\sin i$ .

439 our general conclusions on survey parameters and viability. They can, however, greatly affect the  
440 achievable sensitivity for any specific star. Simulations that consider those additional features may be  
441 needed to more tightly define targets, especially for specific (as opposed to our generic) instruments.

### 442 9.3. *Dispatch Scheduler considerations*

443 Exposure times, stellar positions, site weather, and how targets are chosen all affect observation  
444 counts. Our time since last-observed weighting minimizes RA shadowing issues, so target spacing is  
445 not an overly large concern.

446 More generally, the dispatch scheduler deals relatively well with distributing observations between  
447 different targets, getting as many observations for each target as possible, and dealing gracefully with  
448 targets being difficult to observe. This combination of “good enough” and being computationally  
449 cheap is why we do not look at other weighting options, or more complicated algorithms such as  
450 Garcia-Piquer et al. (2017)

451 The “Traveling Telescope Problem” (Handley et al. 2024a) and associated slew concerns are pri-  
452 marily for the short exposure limit. The sorts of exposure times that we have here (including with  
453 the p-mode compensation) suggest that we would have fewer observations per hour/per night than  
454 they would. However, our assumed slew times are intentionally conservative, so work such as this  
455 could improve upon our assumptions.

456 Exploring how much of an improvement is possible with these sorts of methods, and if they present  
457 other limitations would be an avenue for future research.

458

#### 9.4. Target Weighting

459

Number of observations per star were looked at for weighting schemes based on hour angle and/or time since last observation (with minimum delays between observations of 0.5, 1, 2, 4, 8, 16, and 32 hours considered). Variants on relative weighting strength were not otherwise attempted. Due to the difficulties in comparing histograms, the mean, median, and standard deviation of the number of observations were considered as figures of merit.

460

461

462

463

464

465

466

467

In general, target selection (number of stars, exposure times, location) had larger effects than the algorithms explored. Which weighting algorithm was more effective also depended on the target list. A small/widely separated one did best with pure hour angle. The full list contains a number of stars that can interfere with each-other, so a method of upweighting that prevents that is preferred.

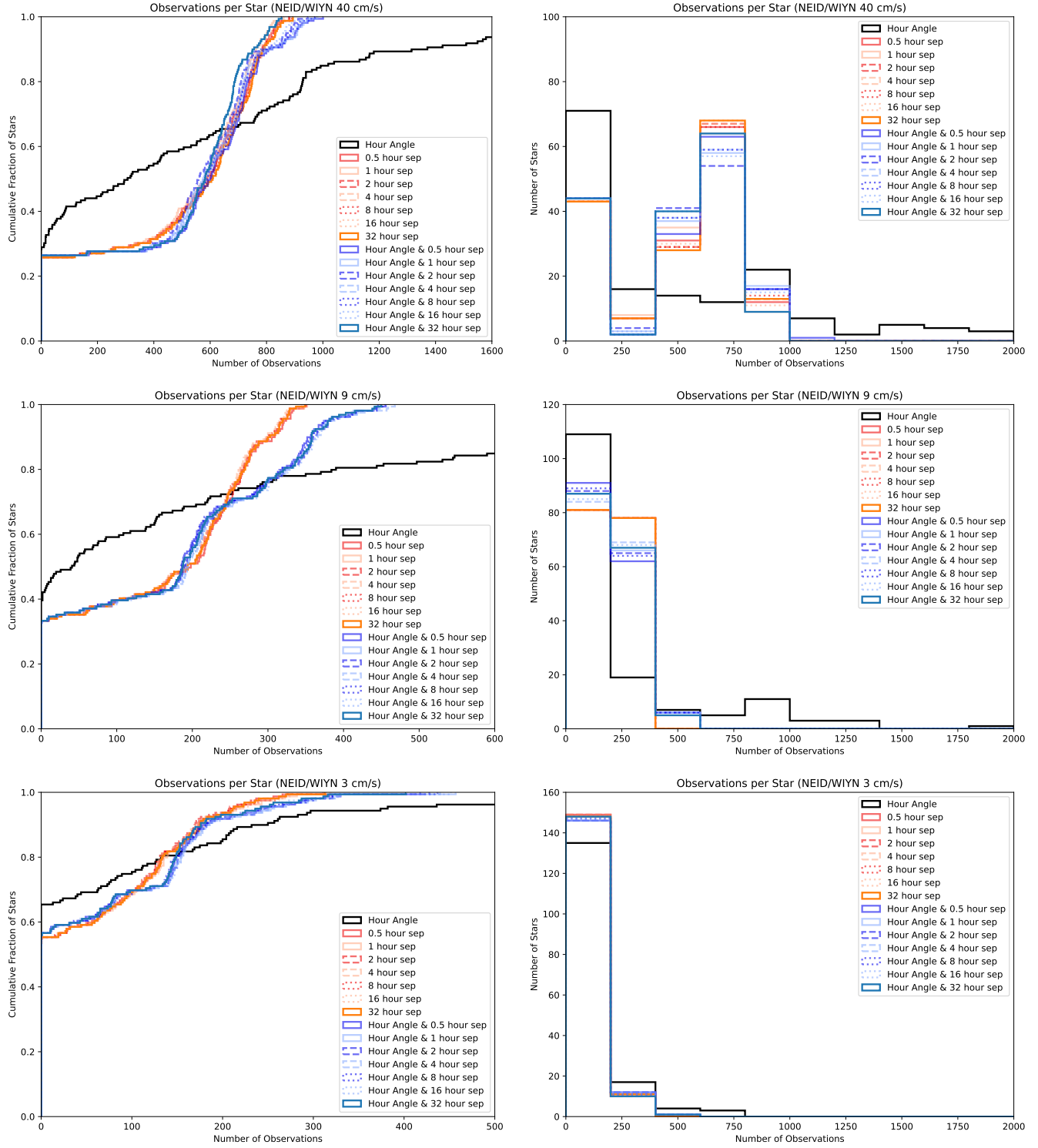


**Figure 22.** PDFs (left), and CDFs (right) of all stars in the HWO target list for different precisions and a large variety of observation weighting strategies. Here we look at 3 main strategies: a simplistic hour-angle weighting, a time since last observation weighting (do not observe the object again at all within the time limit, and then ramp up the weighting), and a combined hour-angle and time since last observation weighting. The last two are relatively similar (especially for shorter exposure times), but we find that the combined weighting is the “best”.

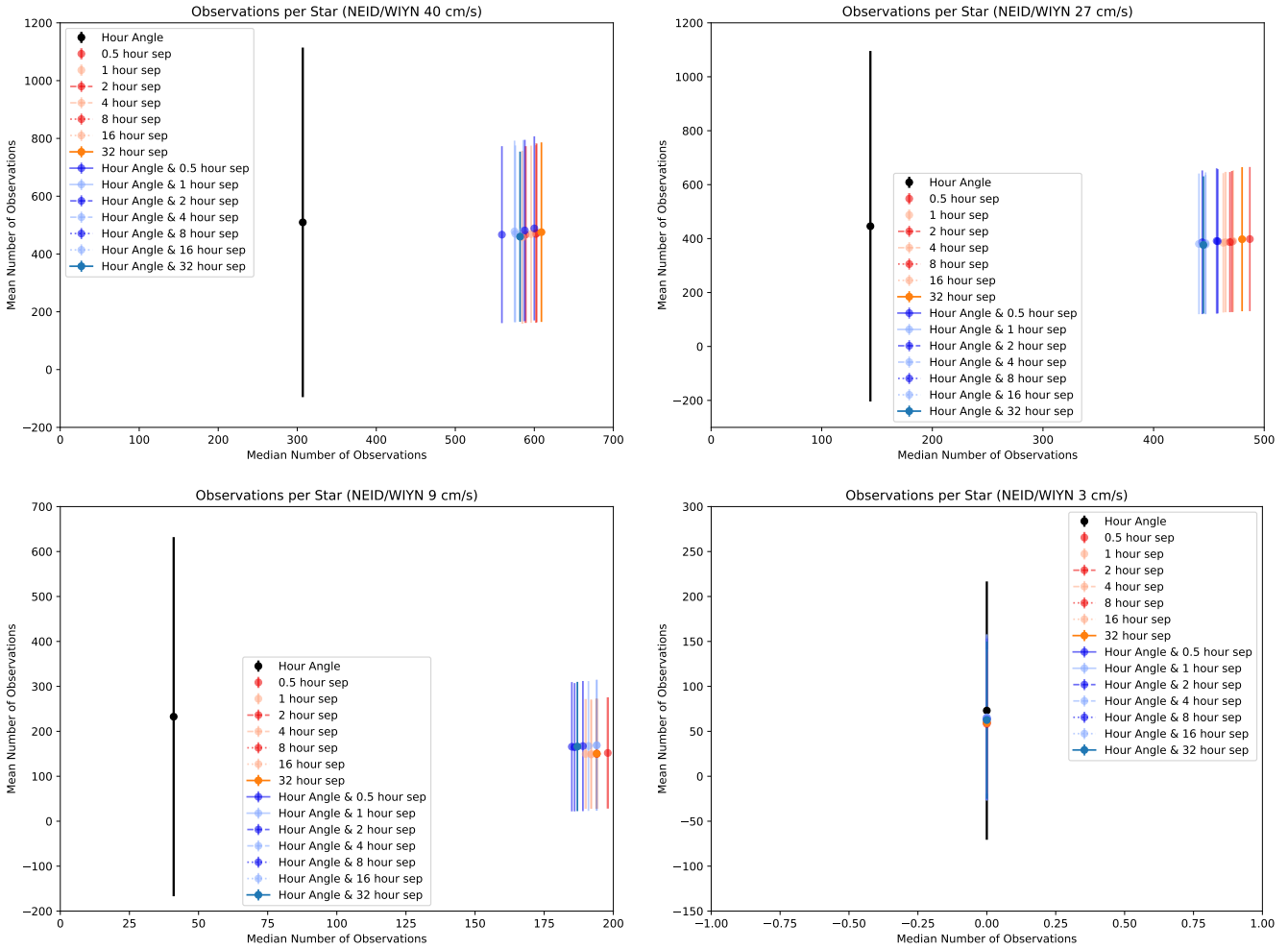


**Figure 23.** Plots of the distribution of results for different precisions and a variety of weighting strategies. We compare median (x-axis) with mean (y-axis) and standard deviation (error bars). Here we look at 3 main strategies: a simplistic hour-angle weighting, a time since last observation weighting (do not observe the object again at all within the time limit, and then ramp up the weighting), and a combined hour-angle and time since last observation weighting. The last two are relatively similar (especially for shorter exposure times), and unlike the broader distributions, it looks like pure time since last observation is the “best”. Notably, for 3 cm/s, we are unable to observe the majority of the stars, hence a median of 0.

### 9.5. Do the different P-mode calculation methods affect yields?

The minimum timescale as determined by the p-mode oscillations has a large effect on exposure times only when other factors combine to result in very short exposures. They set a floor which within our constraints is only reached for relatively low precisions, favorable stars, and/or large telescopes.

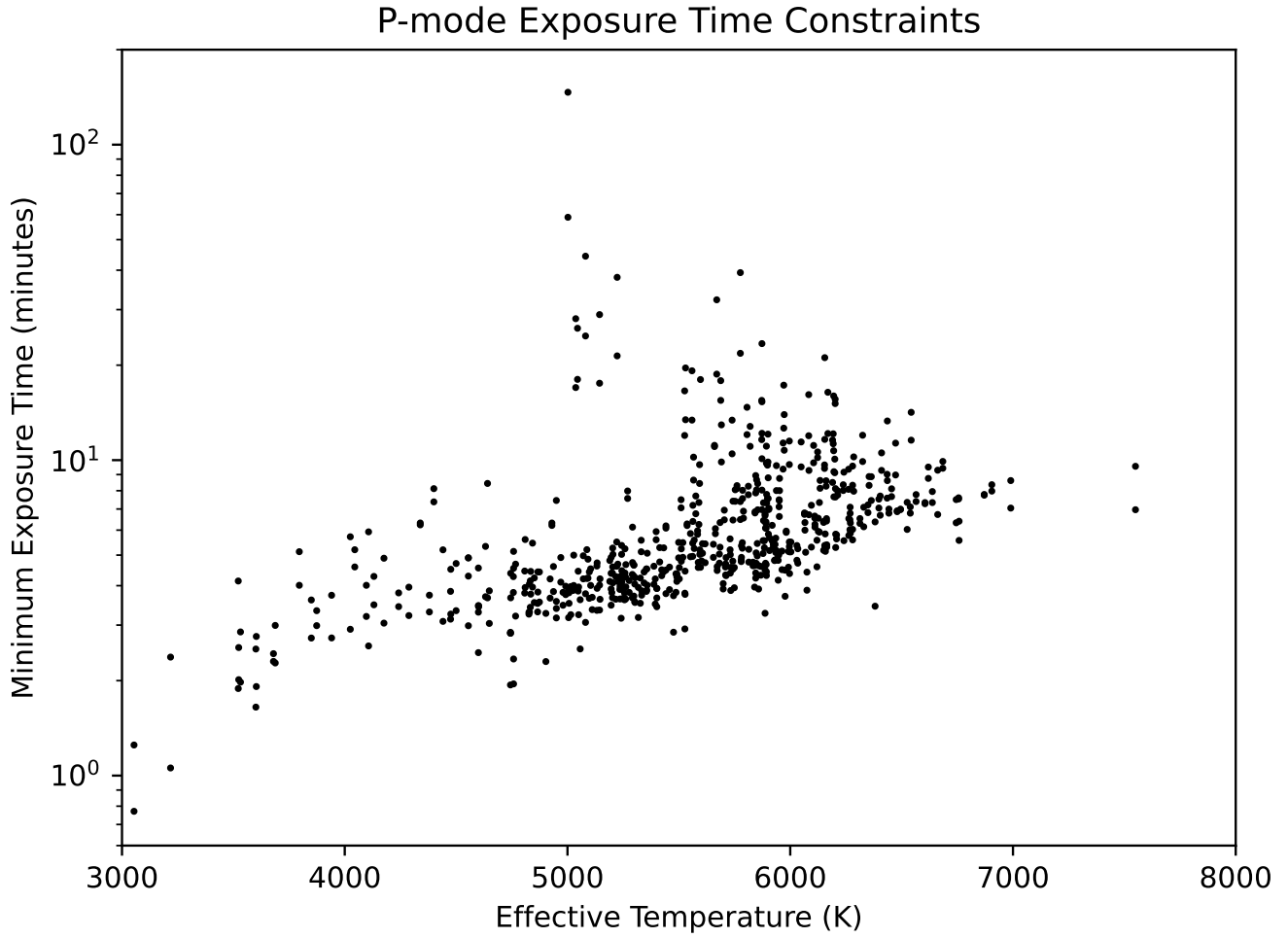


**Figure 24.** All minimum p-mode times across all target lists as a function of effective temperature. Most are shorter than 5 minutes and the vast majority are shorter than 10. The remainder include stars that a direct observation mission may wish to pass over (eg: subgiants).

472 While both the mass-radius and gravity-temperature methods look similar, it is worthwhile to  
 473 check to see if they are producing different distributions. To do this, we performed K-S tests on  
 474 our distributions of exposure times, observation counts, and K/SNR heuristics. We first look at the  
 475 extremes of short and long exposure time cases that we simulated, and then at the shortest ones  
 476 within the preferred instrument/telescope/sensitivity combinations.

477 While we do see some differences, the shortest exposure time we simulated is a “noncanonical”  
 478 telescope/instrument combination with a telescope size and instrument sensitivity that is at the edge  
 479 of the trade-space. The shortest exposure time combination that is “canonical” (27 cm/s NEID  
 480 analog on a 3.5 m telescope) shows a somewhat different pattern.

481 Any physically-motivated p-mode comparison appears to have similar effects on survey results for  
 482 a realistic survey, though differences are possible in the short-exposure limit. If a survey spends a  
 483 relatively long time on each star, then the method will not matter.

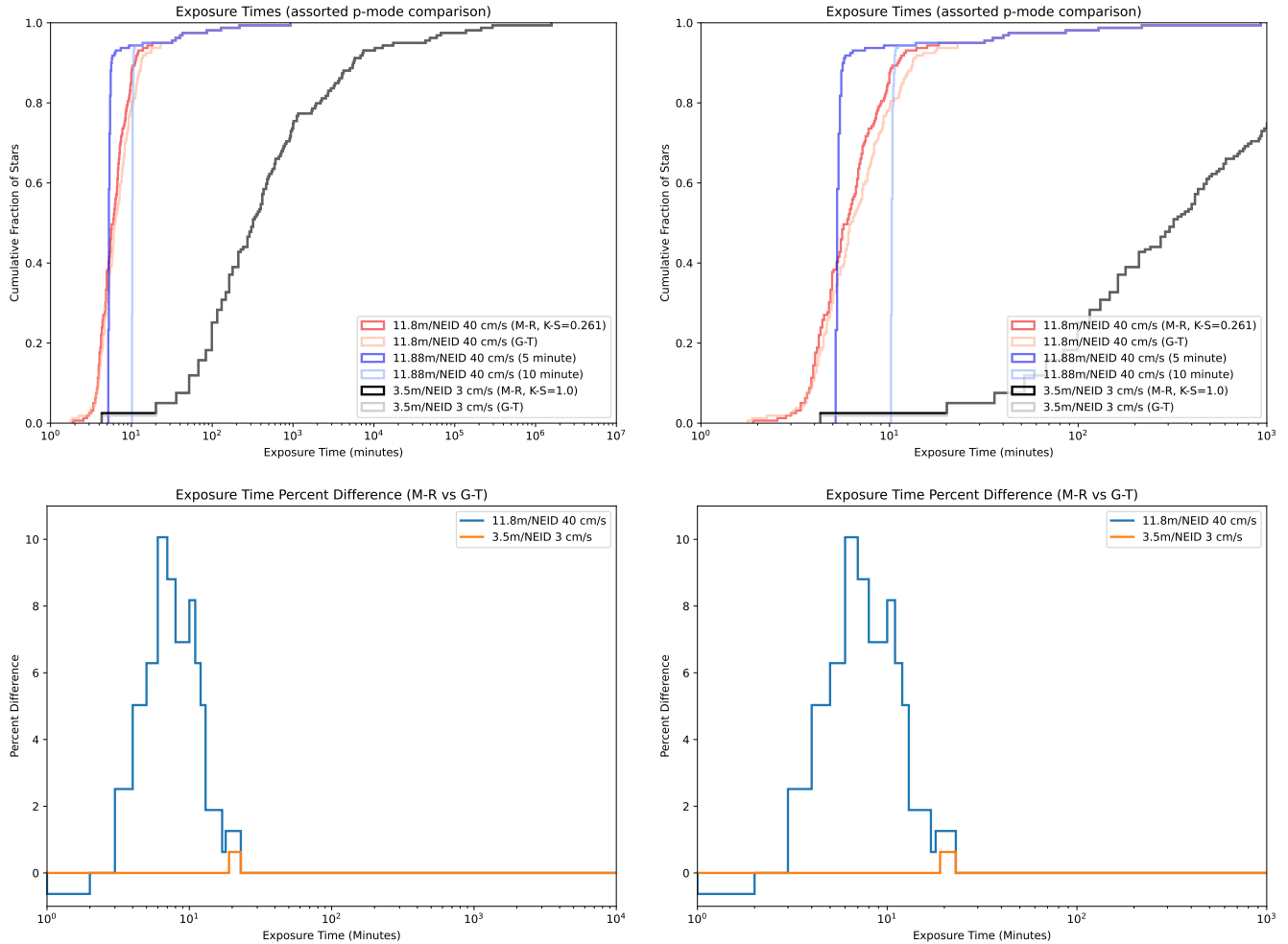


**Figure 25.** Comparison of the exposure time distributions for four kinds of p-mode oscillation compensation measures: fixed 5-minute versus fixed 10-minute versus two kinds of variable (mass-radius and effective temperature-surface gravity). The telescope/precision combinations that otherwise give the shortest exposures (11.8 m and 40 cm/s) and longest exposures (3.5 m and 3 cm/s) using NEID are used. In the CDF graphs (**top**), the p-values for a null result between the two variable exposure modes (the mass-radius and temperature-gravity using distributions are the same) are given in the figure keys. The **bottom** panels show 'percent difference' between the two variable p-mode timescale distributions. The two fixed timescale distributions are not considered, as they are different by inspection (though overlap in some ways with the other distributions). The K-S test does not show these two distributions as statistically different (the p-value for the 40 cm/s case is >0.05, and for the 3 cm/s case is around 1).

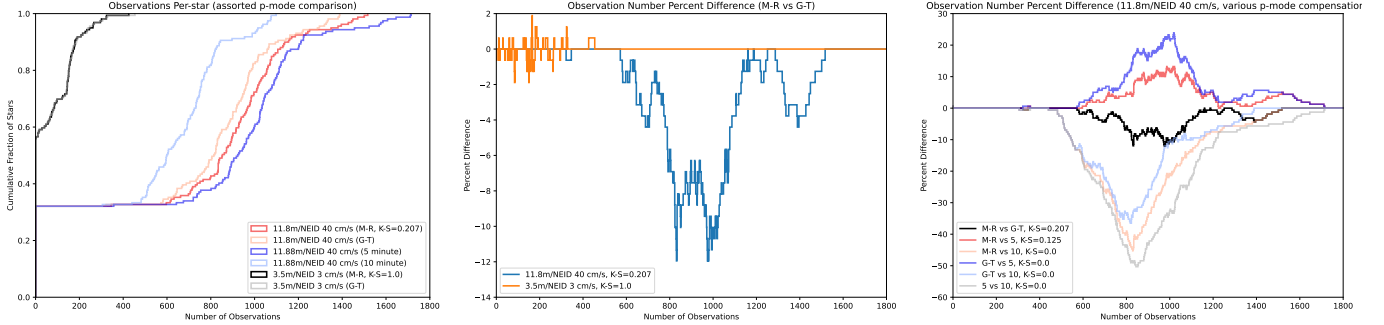


**Figure 26.** Comparison of the same 6 datasets in observation distribution. The left graph is the CDF of the distributions, while the middle is the percent difference for the two variable p-modes, and the right is the percent difference between all combinations for the short exposure time case. Notably unlike the exposure time distributions, these are in some cases distinguishable from each-other.

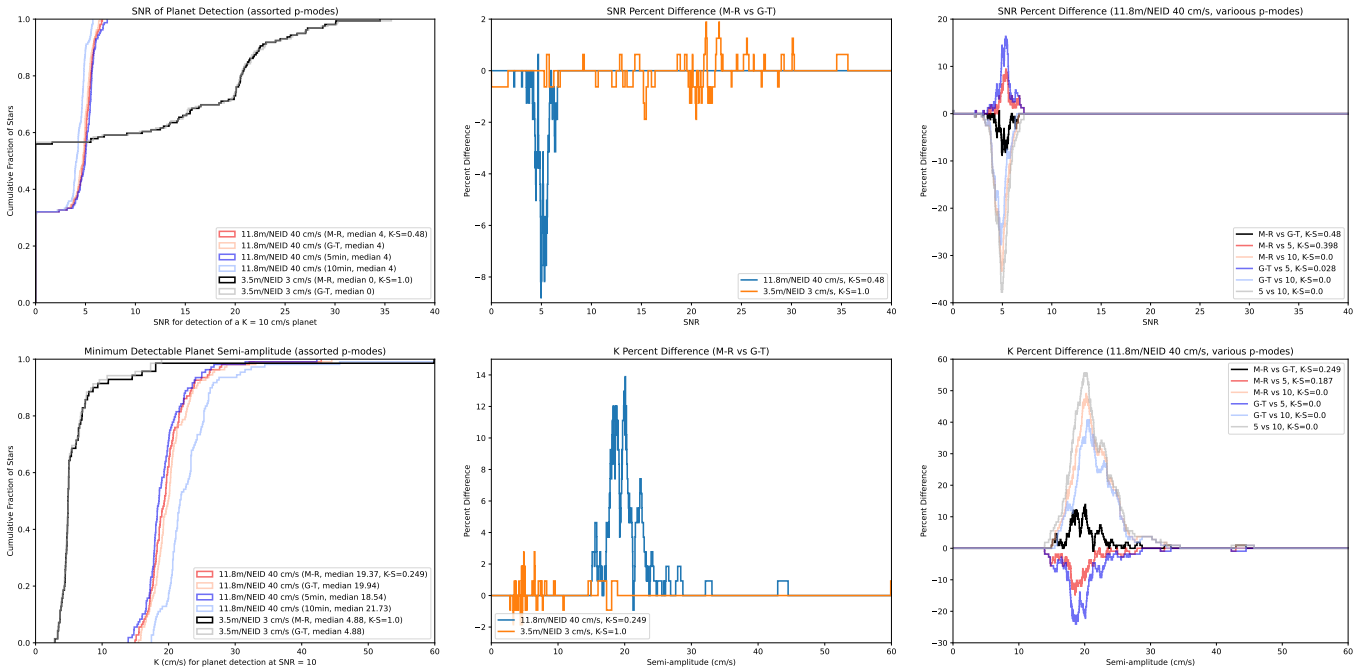


**Figure 27.** Comparison of the same 6 datasets in their distributions for our K/SNR detection heuristic (semi-amplitude sensitivity at an SNR of 10 is top, SNR for a fixed semi-amplitude of 10 cm/s is bottom). The left graphs are the CDF of the distributions, while the middle are the percent difference for the two variable p-modes, and the right is the percent difference between all combinations for the short exposure time case. Using a cutoff of  $p < 0.05$ , we find that the two variable p-mode calculations cannot be distinguished from each-other, nor the mass-radius method from a 5-minute cutoff. All others can be, as can usually be seen by offsets in their CDFs (which appear as peaks/troughs in the percent difference).

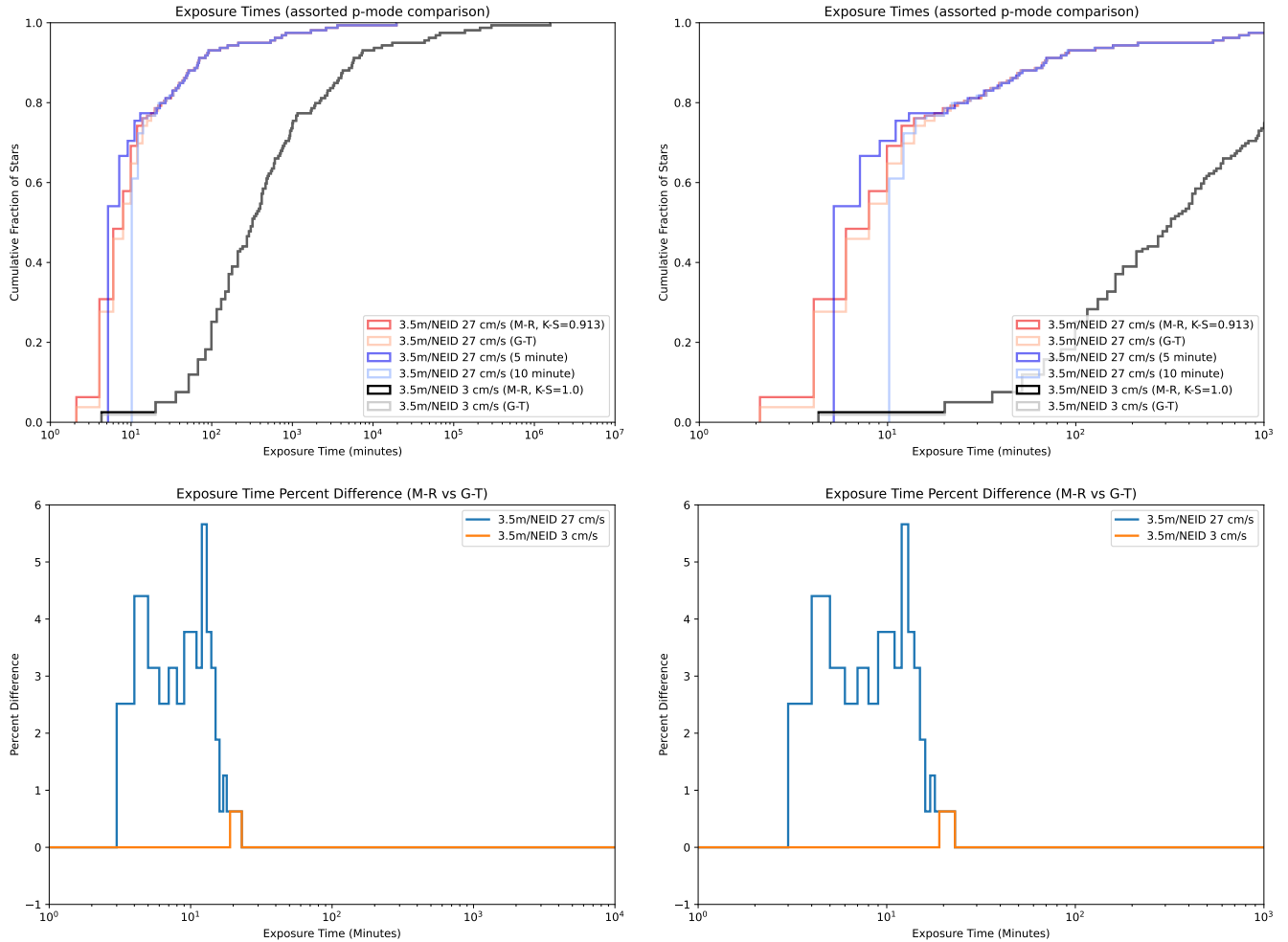


**Figure 28.** Comparison of the exposure time distributions for four kinds of p-mode oscillation compensation measures: fixed 5-minute versus fixed 10-minute versus two kinds of variable (mass-radius and effective temperature-surface gravity). The telescope/precision combinations that are “canonical” and give the shortest exposures (3.5 m and 27 cm/s) and longest exposures (3.5 m and 3 cm/s) using NEID are used. In the CDF graphs (**top**), the p-values for a null result between the two variable exposure modes (the mass-radius and temperature-gravity using distributions are the same) are given in the figure keys. The **bottom** panels show ‘percent difference’ between the two variable p-mode timescale distributions. The two fixed timescale distributions are not considered, as they are different by inspection (though overlap in some ways with the other distributions). The K-S test does not show these two distributions as statistically different (with p-values of near to or exactly 1).

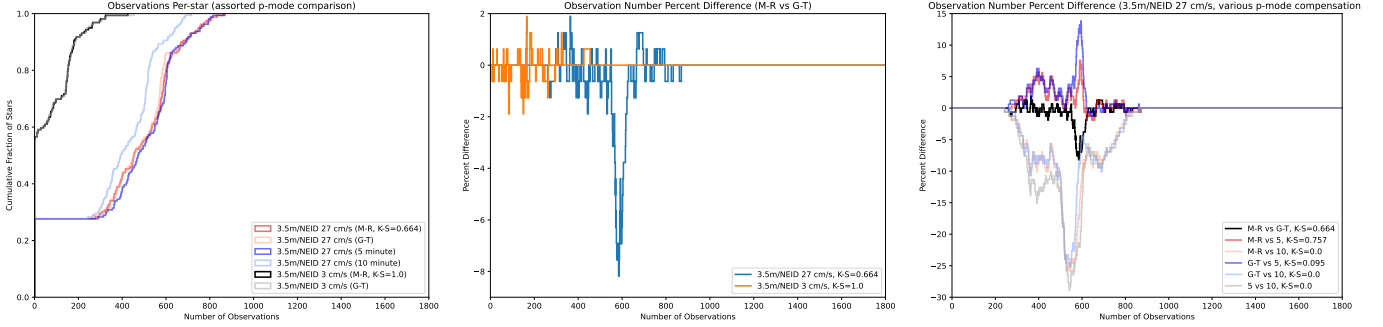


**Figure 29.** Comparison of the same 6 datasets in observation distribution. The left graph is the CDF of the distributions, while the middle is the percent difference for the two variable p-modes, and the right is the percent difference between all combinations for the short exposure time case. The variable p-modes remain indistinguishable from each-other, though the fixed 5-minute is somewhat distinguishable from either. The fixed 10-minute p-mode has a statistically significant and visible offset distribution from the rest.

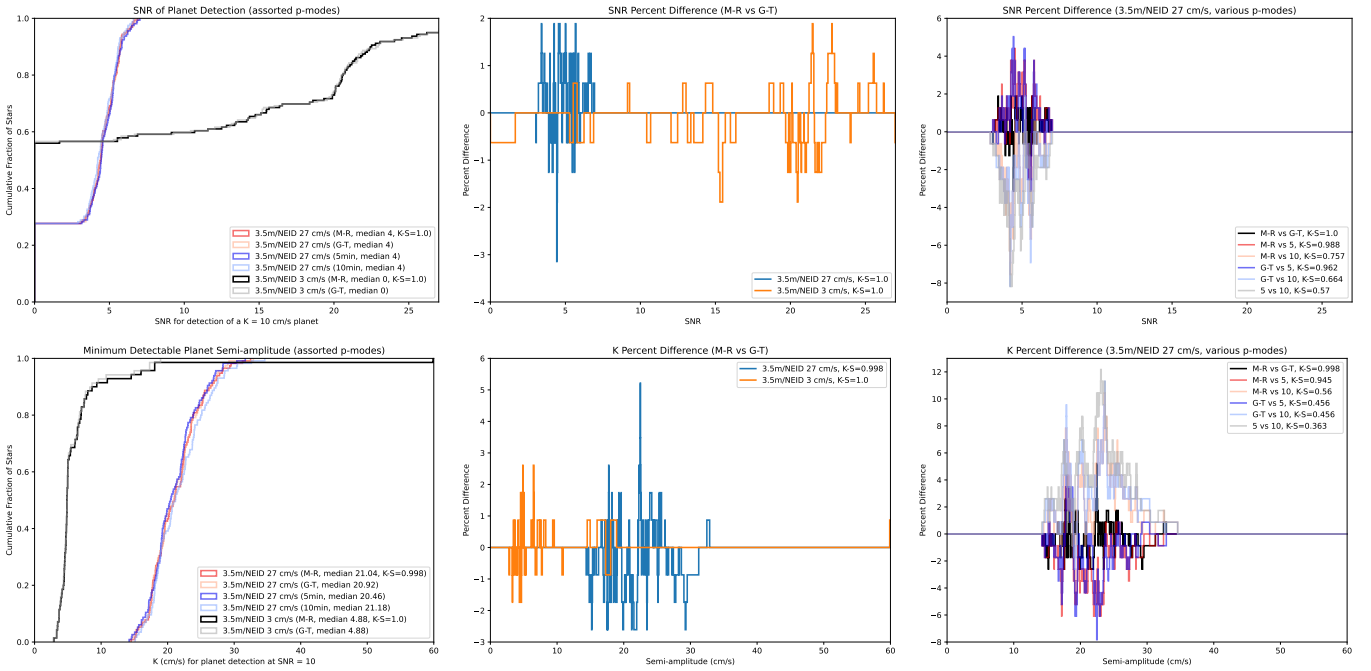


**Figure 30.** Comparison of the same 6 datasets in their distributions for our K/SNR detection heuristic (semi-amplitude sensitivity at an SNR of 10 is top, SNR for a fixed semi-amplitude of 10 cm/s is bottom). The left graphs are the CDF of the distributions, while the middle are the percent difference for the two variable p-modes, and the right is the percent difference between all combinations for the short exposure time case. Using a cutoff of  $p < 0.05$ , we find no p-mode compensation method is different from any other. This is supported by the overlapping CDFs.

484     Exact details of stellar position are likely to be interacting with the changes in exposure times  
485     and/or differences in the weather used (we do not use the same seed for each run), to cause the  
486     differences in the observation distributions. That the flat 5-minute floor produces similar results to  
487     the variable minimum observation times is potentially interesting, though it may be a result of our  
488     assumptions (which give the sun a 300 second, or a 322 second minimum, depending on the method  
489     used).

490     Our detection heuristic has tighter offsets between the CDFs, though due to their near-vertical  
491     portion, these are often statistically significant. These suggest that depending on how it is performed,  
492     our simulations may have systematic errors from p-mode compensation of up to some tens of percent.

493     All of these differences are minimized for telescope/instrument/precision combinations that push  
494     exposure times longer, and can render them of minor importance for some and no importance for a  
495     few of them.

#### 496                 9.6. Target List Comparison/Target Star Selection

497     The choice of target stars dramatically affects survey efficiency and efficacy, primarily through  
498     exposure time and positional constraints. While our code can deal with some difficult to  
499     observe stars, typically due to declination or exposure time, others are impossible to observe at the  
500     sorts of precisions necessary to find earth-analogs. Our stellar activity considerations do not greatly  
501     affect exposure times, so the variations here are primarily about the information content of spectra  
502     and raw number of photons.

503     While in principle our target list is a volume-limited sample, there are sufficiently many stars that  
504     selecting for “easier” ones remains a possibility. Since our most-disfavored stars (hotter ones) are  
505     relatively rare, this does not overly constrain us on number of targets. Focusing on “easier” stars  
506     may more subtlety bias the survey, though it still reduces the time an eventual direct imaging survey  
507     needs to spend on detection/allows more focus on classification.

508     As we find that an optimistic declination cut does not present issues, this suggests that they should  
509     be chosen more on limiting the number of target stars (assuming that there are too many with short  
510     exposure times) than by constraints on observability.

511     Stars with limited numbers of observations would risk having alias issues. A more subtle aspect  
512     of our assumptions is that we want a high cadence to properly model stellar activity. While these  
513     simulations use a single site, weather losses (and potentially target list size) would introduce gaps  
514     could make this level of activity characterization impossible.

515     As we have multiple nominally optimized target lists, we can do a degree of comparison.

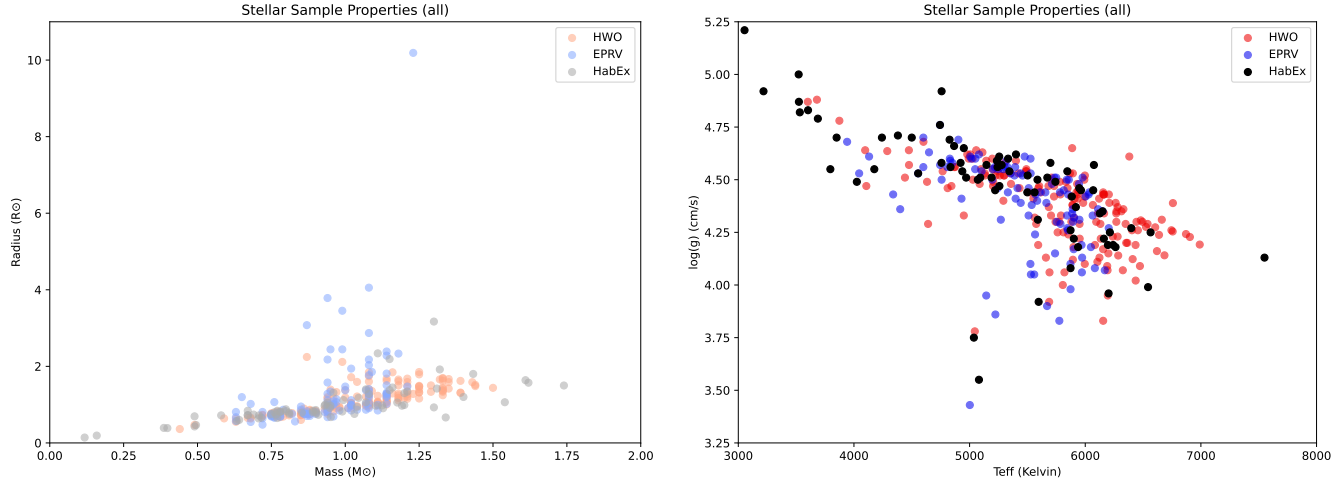


**Figure 31.** A comparison of our 3 target lists in the parameter spaces used for p-mode compensation.

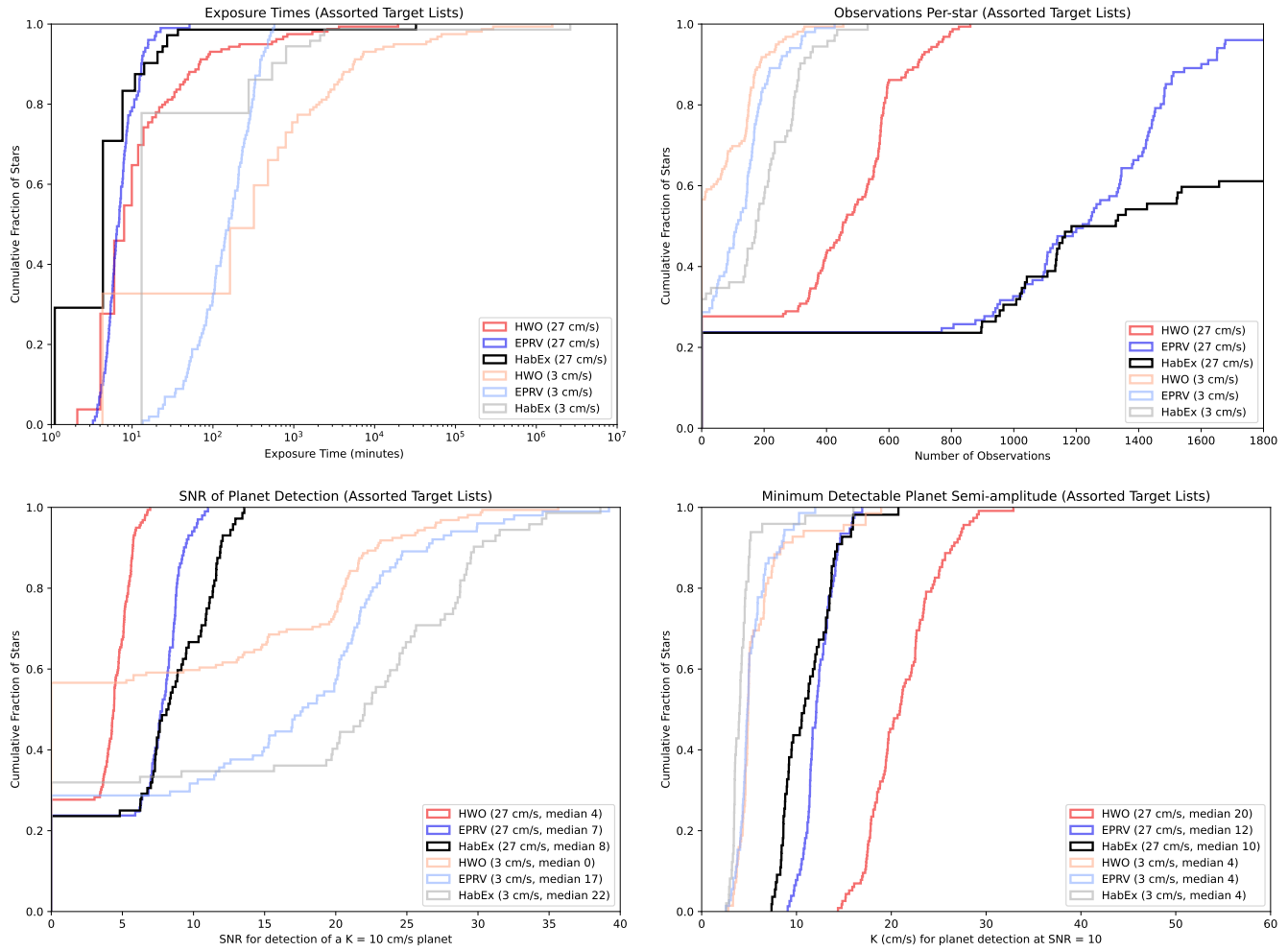


**Figure 32.** A comparison of our 3 target lists (HWO, EPRV, HabEx), for typical high and low precisions using the NEID spectrograph on a 3.5 m telescope. (**top:** CDFs of exposure times and observation counts, **bottom:** CDFs of our K/SNR detection heuristic).

The apparent differences are likely caused by these CDFs glossing over the differing sizes of the target lists, as well as the differing observability. The increased number of stars in general, and “good” stars in particular the HWO list (as compared with the HabEx and EPRV lists) means that observations are spread out over more stars, and everything gets measured to a lower precision.

While we do not quantify the value of target list size (aside from our detection heuristic), this suggests a limit to the target list length for a precursor survey, especially with the large number of observations required. If a survey is to be volume limited, it may need more or larger telescopes to get sufficient numbers.

If our primarily unmodeled noise sources are white noise (as our detection heuristic assumes), this does point to a smaller / more frequently observed target list as a way to compensate for noise sources that are otherwise larger than we consider.

### 9.7. Other/Uncompensated Noise

We do not attempt to directly mitigate any noise beyond oscillations, likely resulting in significant reductions in ‘actual’ SNR values and higher minimum semi-amplitudes than are shown. (Though longer exposures also likely suffer less from granulation.) Using Luhn et al. (2023)’s results as a figure of merit, we expect reductions on the order of a factor of 3-6 for correlated noise, and 2 for white noise, for a total reduction in SNR of about 4-9x. There is a great deal of ongoing work to improve on stellar activity, including sun as a star observations. (Rubenzahl et al. 2023; Llama et al. 2024; Ford et al. 2024; Klein et al. 2024) These suggest that a NEID-equivalent could find an Earth-analogue around a sun-analogue with on the order of 1000 observations, a number that we reach for many targets. Additional work to mitigate noise may be able to reduce these further, and more realistic simulations of both the noise sources and mitigations thereof would be work for a future paper.

Finally, we do not attempt to model telluric noise, assuming that it will be sufficiently small and/or there will be improvements in mitigation/modeling. Our nominal noise parameters suggest that this is a safe assumption in the visible, but not in the infrared (from their sizes relative to other noise sources). While upcoming EPRV observatories (and the nominal instruments we simulate) will have features like sky fibres, more work is needed.

## 10. CONCLUSIONS

We (re)introduce a series of codes for calculating exposure times/RV precision, taking into account some degree of atmospheric absorption and compensating for some stellar activity. We also (re)introduce codes for performing realistic dedicated surveys.

We consider multiple target weighting algorithms, settling on a combination of hour angle and time since last observation. Despite the simplicity, does a relatively good job of making use of the telescope and distributing observations among target stars, with results in line with real-world surveys.

We compare the code with existing exposure time calculators and find (results) broadly similar temperature trends. What parameters various ETCs consider varies enough that other comparisons are difficult, and suggest serious limits on their accuracy without careful per-site/instrument or per-target adjustments. However, our broad trends should be sufficient for “typical” targets.

The importance of cadence/multiple sites is highlighted for avoiding poor detection strength from weather.

We have found that target star selection is important for reasons above and beyond stellar activity. eg: Slow-rotating nearby K-dwarfs are much easier to observe than many others. Early M-dwarfs

may also work well. G-dwarfs, while more difficult are doable. F and especially A stars are impractical to obtain our desired single measurement precision on. These effects are from: effective temperature being comparatively unimportant over a wide range, but reducing line quantity and increasing microturbulence for hotter stars, as well as increasing rotational velocities (especially past the Kraft Break).

Target star declination is important, though like effective temperature has a relatively broad range where stellar observations are similar in difficulty and number. Right ascension can also matter, though how much and which ones are “best” will vary with the site (from weather and length of night). Even for the “worst” right ascensions, a target list should have some stars, unless exposure times are so long that the list needs to have a minimum of targets.

While previous work showed that one can account for p-mode oscillations approximately (and that they don’t necessarily affect survey results), we show that we can also directly choose exposure times to minimize them. This does not present significant computational overhead or increase in survey difficulty, and so can “just” be done in future EPRV work.

We also show that the p-mode compensation method has little effect on exposure times (and therefore observation rates), outside of the large telescope/low precision limit. The physically based methods use related scaling methods and are centered at solar ( 5 minute) values, so this is unsurprising. An intentionally different method (10 minutes) does offset things, but again the effect is small and only relevant when exposure times are short (well below 10 minutes).

Finally, we find that telluric noise sources are presently manageable in the visible, but are showstoppers in the NIR without additional corrections.

*Software:* astropy (The Astropy Collaboration et al. 2018a) (The Astropy Collaboration et al. 2018b) numpy (Oliphant 2006) matplotlib (Hunter 2007)

## REFERENCES

- Adelman, S. J. 2004, in The A-Star Puzzle, ed. J. Zverko, J. Ziznovsky, S. J. Adelman, & W. W. Weiss, Vol. 224, 1–11
- Ammler-von Eiff, M., & Reiners, A. 2012, A&A, 542, A116
- Batalha, N. E., Kempton, E. M. R., & Mbarek, R. 2017, ApJL, 836, L5
- Batalha, N. E., Lewis, T., Fortney, J. J., et al. 2019, ApJL, 885, L25
- Beatty, T. G., & Gaudi, B. S. 2015, PASP, 127, 1240
- Bergsten, G. J., Pascucci, I., Hardegree-Ullman, K. K., et al. 2023, AJ, 166, 234
- Bergsten, G. J., Pascucci, I., Mulders, G. D., Fernandes, R. B., & Koskinen, T. T. 2022, AJ, 164, 190
- Blackman, R. T., Fischer, D. A., Jurgenson, C. A., et al. 2020, AJ, 159, 238
- Boffin, H. M. J., Vinther, J., Bazin, G., et al. 2024, arXiv e-prints, arXiv:2407.02972
- Bonfils, X., Delfosse, X., Udry, S., et al. 2013, A&A, 549, A109
- Bottom, M., Muirhead, P. S., Johnson, J. A., & Blake, C. H. 2013, PASP, 125, 240
- Boyajian, T. S., McAlister, H. A., van Belle, G., et al. 2012, ApJ, 746, 101
- Brewer, J. M., Fischer, D. A., Valenti, J. A., & Piskunov, N. 2016, The Astrophysical Journal Supplement Series, 225, 32
- Bryson, S., Coughlin, J., Batalha, N. M., et al. 2020, AJ, 159, 279
- Bryson, S., Kunimoto, M., Kopparapu, R. K., et al. 2021, AJ, 161, 36
- Bryson, S., Kunimoto, M., Belikov, R., et al. 2025, arXiv e-prints, arXiv:2511.05658
- Burke, C. J., Christiansen, J. L., Mullally, F., et al. 2015, ApJ, 809, 8
- Changeat, Q., Keyte, L., Waldmann, I. P., & Tinetti, G. 2020, ApJ, 896, 107

- 620 Chaplin, W. J., Cegla, H. M., Watson, C. A.,  
 621 Davies, G. R., & Ball, W. H. 2019, AJ, 157, 163  
 622 de Wit, J., & Seager, S. 2013, Science, 342, 1473  
 623 Demory, B. O., Ségransan, D., Forveille, T., et al.  
 624 2009, A&A, 505, 205  
 625 Dong, S., & Zhu, Z. 2013, ApJ, 778, 53  
 626 Dressing, C. D., & Charbonneau, D. 2015, ApJ,  
 627 807, 45  
 628 Dulz, S. D., Plavchan, P., Crepp, J. R., et al.  
 629 2020, ApJ, 893, 122  
 630 Edvardsson, B., Andersen, J., Gustafsson, B.,  
 631 et al. 1993, A&A, 275, 101  
 632 Fernandes, R. B., Johnson, S., Bergsten, G. J.,  
 633 et al. 2025, arXiv e-prints, arXiv:2511.05660  
 634 Ford, E. B., Bender, C. F., Blake, C. H., et al.  
 635 2024, arXiv e-prints, arXiv:2408.13318  
 636 Foreman-Mackey, D., Hogg, D. W., & Morton,  
 637 T. D. 2014, ApJ, 795, 64  
 638 Garcia-Piquer, A., Morales, J. C., Ribas, I., et al.  
 639 2017, A&A, 604, A87  
 640 Garrett, D., Savransky, D., & Belikov, R. 2018,  
 641 PASP, 130, 114403  
 642 Gáspár, A., Rieke, G. H., & Ballering, N. 2016,  
 643 ApJ, 826, 171  
 644 Gaudi, B. S., & Winn, J. N. 2007, ApJ, 655, 550  
 645 Gaudi, B. S., Seager, S., Mennesson, B., et al.  
 646 2018, arXiv e-prints, arXiv:1809.09674  
 647 Glebocki, R., & Gnacinski, P. 2005, VizieR Online  
 648 Data Catalog, III/244  
 649 Halverson, S., Terrien, R., Mahadevan, S., et al.  
 650 2016, in Society of Photo-Optical  
 651 Instrumentation Engineers (SPIE) Conference  
 652 Series, Vol. 9908, Ground-based and Airborne  
 653 Instrumentation for Astronomy VI, ed. C. J.  
 654 Evans, L. Simard, & H. Takami, 99086P  
 655 Handley, L. B., Petigura, E. A., & Mišić, V. V.  
 656 2024a, AJ, 167, 33  
 657 Handley, L. B., Petigura, E. A., Mišić, V. V.,  
 658 Lubin, J., & Isaacson, H. 2024b, AJ, 167, 122  
 659 Hojjatpanah, S., Figueira, P., Santos, N. C., et al.  
 660 2019, A&A, 629, A80  
 661 Houdebine, E. R. 2010, MNRAS, 407, 1657  
 662 Howard, A. W., & Fulton, B. J. 2016, PASP, 128,  
 663 114401  
 664 Hsu, D. C., Ford, E. B., Ragozzine, D., & Ashby,  
 665 K. 2019, AJ, 158, 109  
 666 Hunter, J. D. 2007, Computing in Science &  
 667 Engineering, 90  
 668 Jurgenson, C., Fischer, D., McCracken, T., et al.  
 669 2016, in Society of Photo-Optical  
 670 Instrumentation Engineers (SPIE) Conference  
 671 Series, Vol. 9908, Ground-based and Airborne  
 672 Instrumentation for Astronomy VI, ed. C. J.  
 673 Evans, L. Simard, & H. Takami, 99086T  
 674 Kaltenegger, L., & Traub, W. A. 2009, ApJ, 698,  
 675 519  
 676 Kaminski, A., Sabotta, S., Kemmer, J., et al.  
 677 2025, A&A, 696, A101  
 678 Kiraga, M., & Stepień, K. 2007, AcA, 57, 149  
 679 Klein, B., Aigrain, S., Cretignier, M., et al. 2024,  
 680 MNRAS, 531, 4238  
 681 Koleva, M., & Vazdekis, A. 2012, A&A, 538, A143  
 682 Kopparapu, R. K. 2013, ApJL, 767, L8  
 683 Kopparapu, R. K., Hébrard, E., Belikov, R., et al.  
 684 2018, ApJ, 856, 122  
 685 Kunder, A., Kordopatis, G., Steinmetz, M., et al.  
 686 2017, AJ, 153, 75  
 687 Kunimoto, M., & Matthews, J. M. 2020, AJ, 159,  
 688 248  
 689 Llama, J., Zhao, L. L., Brewer, J. M., et al. 2024,  
 690 arXiv e-prints, arXiv:2407.07967  
 691 Luck, R. E. 2017, AJ, 153, 21  
 692 Luhn, J. K., Ford, E. B., Guo, Z., et al. 2023, AJ,  
 693 165, 98  
 694 Mamajek, E., & Stapelfeldt, K. 2023, in American  
 695 Astronomical Society Meeting Abstracts,  
 696 Vol. 55, American Astronomical Society  
 697 Meeting Abstracts, 116.07  
 698 Mamajek, E., & Stapelfeldt, K. 2024, arXiv  
 699 e-prints, arXiv:2402.12414  
 700 Mann, A. W., Feiden, G. A., Gaidos, E., Boyajian,  
 701 T., & von Braun, K. 2015, ApJ, 804, 64  
 702 Martínez-Arnáiz, R., Maldonado, J., Montes, D.,  
 703 Eiroa, C., & Montesinos, B. 2010, A&A, 520,  
 704 A79  
 705 Mayor, M., & Queloz, D. 1995, Nature, 378, 355  
 706 Mulders, G. D., Pascucci, I., Apai, D., & Ciesla,  
 707 F. J. 2018, AJ, 156, 24  
 708 Nava, C., Johnson, S., McCrady, N., & Minerva.  
 709 2015, in American Astronomical Society  
 710 Meeting Abstracts, Vol. 225, American  
 711 Astronomical Society Meeting Abstracts #225,  
 712 258.26  
 713 Newman, P. D., Plavchan, P., Burt, J. A., et al.  
 714 2023, AJ, 165, 151  
 715 Newton, E. R., Charbonneau, D., Irwin, J., &  
 716 Mann, A. W. 2015, ApJ, 800, 85

- 717 Newton, E. R., Irwin, J., Charbonneau, D., et al.  
 718 2016, *ApJ*, 821, 93
- 719 Oliphant, T. E. 2006, Trelgol Publishing
- 720 Pascucci, I., Mulders, G. D., & Lopez, E. 2019,  
 721 *ApJL*, 883, L15
- 722 Pasinetti Fracassini, L. E., Pastori, L., Covino, S.,  
 723 & Pozzi, A. 2001, *A&A*, 367, 521
- 724 Pepe, F., Cristiani, S., Rebolo, R., et al. 2021a,  
 725 *A&A*, 645, A96
- 726 —. 2021b, *A&A*, 645, A96
- 727 Petigura, E. A., Howard, A. W., & Marcy, G. W.  
 728 2013, *Proceedings of the National Academy of  
 729 Science*, 110, 19273
- 730 Prugniel, P., Soubiran, C., Koleva, M., & Le  
 731 Borgne, D. 2007, arXiv e-prints, astro
- 732 Prugniel, P., Vauglin, I., & Koleva, M. 2011,  
 733 *A&A*, 531, A165
- 734 Rajpurohit, A. S., Reylé, C., Allard, F., et al.  
 735 2013, *A&A*, 556, A15
- 736 Ramírez, I., Allende Prieto, C., & Lambert, D. L.  
 737 2013, *ApJ*, 764, 78
- 738 Rich, E. A., Wisniewski, J. P., McElwain, M. W.,  
 739 et al. 2017, *MNRAS*, 472, 1736
- 740 Rogers, L. A. 2015, *ApJ*, 801, 41
- 741 Rogers, L. A., & Seager, S. 2010, *ApJ*, 712, 974
- 742 Rubenzahl, R. A., Halverson, S., Walawender, J.,  
 743 et al. 2023, *PASP*, 135, 125002
- 744 Salvador, A., Robinson, T. D., Fortney, J. J., &  
 745 Marley, M. S. 2024, *ApJL*, 969, L22
- 746 Schmude, Jr., R. W. 1994, *International  
 747 Amateur-Professional Photoelectric Photometry  
 Communications*, 57, 12
- 749 Schwab, C., Bender, C., Blake, C., et al. 2019, in  
 750 American Astronomical Society Meeting  
 751 Abstracts, Vol. 233, American Astronomical  
 752 Society Meeting Abstracts #233, 408.03
- 753 Seifahrt, A., Stürmer, J., Bean, J. L., & Schwab,  
 754 C. 2018, in *Society of Photo-Optical  
 755 Instrumentation Engineers (SPIE) Conference  
 756 Series*, Vol. 10702, *Ground-based and Airborne  
 757 Instrumentation for Astronomy VII*, ed. C. J.  
 758 Evans, L. Simard, & H. Takami, 107026D
- 759 Seifahrt, A., Bean, J. L., Stürmer, J., et al. 2020,  
 760 in *Society of Photo-Optical Instrumentation  
 761 Engineers (SPIE) Conference Series*, Vol. 11447,  
 762 *Ground-based and Airborne Instrumentation  
 763 for Astronomy VIII*, ed. C. J. Evans, J. J.  
 764 Bryant, & K. Motohara, 114471F
- 765 Silburt, A., Gaidos, E., & Wu, Y. 2015, *ApJ*, 799,  
 766 180
- 767 Soubiran, C., Le Campion, J.-F., Brouillet, N., &  
 768 Chemin, L. 2016, *A&A*, 591, A118
- 769 Swift, J. J., Bottom, M., Johnson, J. A., et al.  
 770 2015, *Journal of Astronomical Telescopes,  
 771 Instruments, and Systems*, 1, 027002
- 772 The Astropy Collaboration, Price-Whelan, A. M.,  
 773 Sipőcz, B. M., et al. 2018a, ArXiv e-prints,  
 774 arXiv:1801.02634
- 775 —. 2018b, *AJ*, 156, 123
- 776 Valenti, J. A., & Fischer, D. A. 2005, *ApJS*, 159,  
 777 141
- 778 Wang, S. X., Latouf, N., Plavchan, P., et al. 2022,  
 779 *AJ*, 164, 211
- 780 Youdin, A. N. 2011, *ApJ*, 742, 38
- 781 Zink, J. K., & Hansen, B. M. S. 2019, *MNRAS*,  
 782 487, 246